THESIS FOR THE DEGREE OF DOCTOR OF PHILOSOPHY

Innovative Oxygen Carriers for Chemical-looping Combustion

DAZHENG JING

CHALMERS

Department of Chemistry and Chemical Engineering
CHALMERS UNIVERSITY OF TECHNOLOGY
Gothenburg, Sweden 2015

Innovative Oxygen Carriers for Chemical-looping Combustion

DAZHENG JING
ISBN 978-91-7597-217-6

Doktorsavhandlingar vid Chalmers tekniska högskola
Ny serie Nr 3898
ISSN 0346-718X

Department of Chemistry and Chemical Engineering
Chalmers University of Technology
SE-412 96 Gothenburg
Sweden
Telephone + 46 (0)31-772 1000

Cover: Scanning electron microscopy images of $CaMn_{0.9}Mg_{0.1}O_{3-\delta}$ oxygen carrier calcined at 1300ºC for 4 h. The particles were collected after test in the batch fluidized bed reactor system.

Chalmers Reproservice
Gothenburg, Sweden 2015

ABSTRACT

Chemical-looping combustion (CLC) and chemical-looping with oxygen uncoupling (CLOU) are combustion technologies where carbon dioxide is inherently obtained in pure form without any gas separation step. In the processes, fuel is introduced to the fuel reactor and combustion air is introduced to the air reactor. Circulating metal oxide particles transport oxygen from the air to the fuel reactor, and high purity CO_2 can be obtained after steam condensation. Some metal oxides have the ability to release oxygen to the gas phase, or so-called uncoupling properties, which may facilitate fuel conversion.

The metal oxide, named oxygen carrier, is the cornerstone of the CLC process. Prior to this work, NiO was the benchmark oxygen carrier for gaseous fuels, like natural gas. However, the high cost, toxicity and thermodynamic limitation of Ni would likely make it difficult to up-scale a process using this type of oxygen carrier. Thus, the focus in this work is on oxygen carriers based on cheaper and more environmentally benign materials, i.e. combined manganese oxides and CuO-based oxygen carriers. Both of these types of oxygen carriers have the propensity to release gas phase oxygen in the fuel reactor, something which was deemed highly beneficial. The main focus is on the combined materials, and this work presents the first major screening of these types of oxygen carriers. All oxygen carriers were manufactured by the commercial spray-drying method and examined in a batch fluidized reactor system with respect to parameters important for chemical-looping.

Several combined manganese oxide systems were investigated in this work, with the main focus on three rather promising systems: i) calcium manganites, ii) manganese-silica and iii) manganese with magnesium. For the first system, Ca-Mn-X-O (X= Fe, Ti and Mg), all materials had perovskite structure and performed very well. Clear oxygen uncoupling ability and full conversion of CH_4 were achieved in the batch testing. Adjusting the production parameters, i.e. calcination temperature, calcination time and milling time, the physical properties of the oxygen carrier can be enhanced. The oxygen carrier with molar composition $CaMn_{0.775}Mg_{0.1}Ti_{0.125}O_{3-\delta}$ was produced by a wide range of Mn- and Ti-sources available commercially at tonnage scales. All materials showed similar oxygen uncoupling behaviour and had the perovskite structure. This shows that this type of oxygen carrier not only can be produced with cheap raw materials, but is simple to produce independent of the material source.

Although the oxygen carriers based on Mn-Si-O had limited oxygen release at lower temperatures, there was a remarkable increase in release at temperatures above 950°C for particles with less than 45 wt% SiO_2. Similarly, the ability to convert CH_4 for these particles increased with temperature, and over 90% combustion could be achieved at temperatures at and above 950°C. The third promising system investigated was a combination of Mn and Mg oxides. In this system, the uncoupling reactions were more pronounced at 900°C for the material with a molar ratio of Mn/Mg of one. Also, the methane conversion for some samples studied was high, making this material yet another interesting alternative.

CuO-based materials with different support materials have a seemingly fast release rate of oxygen, approaching equilibrium at 900°C. Most investigated materials had the ability to fully convert CH_4 at 925°C at the experimental conditions. Some CuO-support combinations did not perform so well, for instance the Cu36FAl24 sample due to formation of $Cu_{0.95}Fe_{1.05}AlO_4$.

Several very promising oxygen carriers have been developed in this work. Some of them have been successfully tested in continuous operation at 120 kW scale. Further, the work has led to the development of calcium manganites ready to be up-scaled to large scale application. In addition to this, several other promising systems have been developed, which may not be ready for upscaling, but have great potential when optimized further.

Keywords: *Chemical-looping combustion, Chemical-looping with oxygen uncoupling, Oxygen carrier, Combined manganese oxides, CuO-based oxygen carrier*

LIST OF PUBLICATIONS

This thesis is based on the work contained in the following papers.

Paper I
T. Mattisson, D. Jing and A. Lyngfelt, *Experimental investigation of binary and ternary combined manganese oxides for chemical-looping with oxygen uncoupling (CLOU),* Submitted for publication.

Paper II
P. Hallberg, D. Jing, M. Rydén, T. Mattisson and A. Lyngfelt, *Chemical Looping Combustion and Chemical Looping with Oxygen Uncoupling Experiments in a Batch Reactor Using Spray-Dried* $CaMn_{1-x}M_xO_{3-\delta}$ *(M = Ti, Fe, Mg) Particles as Oxygen Carriers*, Energy & Fuels, 2013, **27**, 1473–1481.

Paper III
D. Jing, T. Mattisson, M. Rydén, H. Leion and A. Lyngfelt, *Examination of Perovskite Structure* $CaMnO_{3-\delta}$ *with MgO Addition as Oxygen Carrier for Chemical Looping with Oxygen Uncoupling Using Methane and Syngas,* International Journal of Chemical Engineering, vol. 2013, Article ID 679560, 16 pages, 2013.

Paper IV
D. Jing, F. Snijkers, P. Hallberg, H. Leion, T. Mattisson and A. Lyngfelt, *Effect of production parameters on spray dried* $CaMn_{0.9}Mg_{0.1}O_{3-\delta}$ *oxygen carriers,* Submitted for publication.

Paper V
D. Jing, M. Jacobs, P. Hallberg, A. Lyngfelt and T. Mattisson, *Development of* $CaMn_{0.775}Mg_{0.1}Ti_{0.125}O_{3-\delta}$ *oxygen carriers produced using different Mn and Ti sources,* Submitted for publication.

Paper VI
D. Jing, M. Arjmand, T. Mattisson, M. Rydén, F. Snijkers, H. Leion and A. Lyngfelt, *Examination of oxygen uncoupling behaviour and reactivity towards methane for manganese silicate oxygen carriers in chemical-looping combustion,* International Journal of Greenhouse Gas Control, 2014, **29**,70-81

Paper VII
M. Rydén, D. Jing, M. Källén, H. Leion, A. Lyngfelt and T. Mattisson, *CuO-Based Oxygen-Carrier Particles for Chemical-Looping with Oxygen Uncoupling − Experiments in Batch Reactor and in Continuous Operation,* Industrial & Engineering Chemistry Research, 2014, **53**, 6255-6267

Contribution report

I. Responsibility for experimental work, shared responsibility for data evaluation and writing.

II. Shared responsibility for experimental work, data evaluation and writing.

III. Responsible for experimental work, data evaluation and writing.

IV. Responsible for most experimental work, data evaluation and writing.

V. Responsible for experimental work, the majority of data evaluation and writing. The attrition testing and modelling was performed by co-authors.

VI. Responsible for data evaluation and writing. Shared responsibility for experimental work

VII. Responsible for experimental work and data evaluation for experiments conducted in the batch reactor system. Shared responsibility for writing.

Related papers not included in the thesis

- P. Hallberg, M. Källén, D. Jing, F. Snijkers, J. van Noyen, M. Rydén and A. Lyngfelt, *Experimental Investigation of $CaMnO_{3-\delta}$ Based Oxygen Carriers Used in Continuous Chemical-Looping Combustion,* International Journal of Chemical Engineering, vol. 2014, Article ID 412517, 9 pages, 2014.

- F. Snijkers, D. Jing, J. van Noyen, T. Mattisson, M. Jacobs and A. Lyngfelt, *Preparation and properties of perovskite Mn-based oxygen carriers for Chemical Looping Combustion by industrial spray drying method,* the 3rd International Conference on Chemical Looping, Göteborg, Sweden, 2014.

- D. Jing, T. Mattisson, M. Rydén, P. Hallberg, A. Hedayati, J. Van Noyen, F. Snijkers and A. Lyngfelt, *Innovative Oxygen Carrier Materials for Chemical-Looping Combustion*, Energy Procedia, 2013, 37, 645-653.

- G. Azimi, D. Jing, H. Leion and T. Mattisson, *Iron-manganese oxide supported on $MgAl_2O_4$ and ZrO_2 as oxygen carriers for Chemical-Looping with Oxygen Uncoupling,* Proceeding of the 38th International Technical Conference on Clean Coal & Fuel Systems, Clearwater Florida, USA, 2013

- T. Mattisson, D. Jing, G. Azimi, M. Rydén, J. van Noyen and A. Lyngfelt, *Using $(Mn_xFe_{1-x})_2SiO_5$ as oxygen carriers for chemical-looping with oxygen uncoupling (CLOU),* AIChE Annual Meeting, San Francisco, CA, USA, 2013

- M. Rydén, M. Källén, A. Hedayati, D. Jing,T. Mattisson and A. Lyngfelt, *$(Fe_{1-x}Mn_x)Ti_yO_3$ based oxygen carriers for chemical-looping combustion (CLC) and chemical-looping with oxygen uncoupling (CLOU),* the 7th Trondheim CCS Conference, Trondheim, Norway, 2013

- D. Jing, E. Y. S. I. M. Hermans, H. Leion, M. Rydén, T. Mattisson, J. Van Noyen and A. Lyngfelt, *Manganese silica combined oxide as oxygen carrier for chemical-looping combustion,* the 2nd International Conference on Chemical Looping, Darmstadt, Germany, 2012.

TABLE OF CONTENTS

1 Introduction

Fossil fuels are the primary energy sources fuelling our modern society, but the conversion of these fuels result in the release of substantial amounts of CO_2 into the atmosphere every year [1]. These anthropogenic CO_2 emissions are recognized as the biggest contributor to enhanced global warming [2]. The increasing global economy with significant energy demand will likely make fossil fuels remain the main energy source in the forthcoming decades. Thus, to mitigate further climate change caused by global warming, reducing CO_2 emissions from combustion of fossil fuels is a key measure.

One possibility to rapidly reduce CO_2 emissions is to capture the CO_2 produced from combustion or industrial processes, then transport and store the carbon dioxide in closed geological formations. This concept is referred to as Carbon Capture and Storage (CCS) [3], which could mean that fossil fuels can still be used in a transition period while renewable energy sources are gradually being phased into the global energy system.

1.1 Combustion technology with CO_2 capture

In CCS, CO_2 is first separated from other gases and then liquefied to facilitate transportation and storage. The scope of this work is CO_2 capture from combustion in power plants, therefore transportation and storage of the captured CO_2 will not be further discussed, but an overview can be found in IPCC Special Report on Carbon Dioxide Capture and Storage [3].

Generally, combustion technologies with CO_2 capture which are available or under development can be divided into three groups: pre-combustion, post-combustion and oxyfuel combustion. Below follows a short description of each method.

In *pre-combustion,* fuels are first gasified to syngas, a mixture of CO and H_2, in presence of O_2 and/or steam. In the following water-gas shift reactor, CO and steam are converted to CO_2 and H_2 [4]. Prior to combustion in a gas turbine, CO_2 is removed from the hydrogen by chemical or physical absorbents [5]. Though the water-gas shift and CO_2 removal processes applied in this process are commercially applicable, the significant energy consumption for CO_2 separation is an obvious drawback for *pre-combustion*.

Post-combustion is a process where the capture of CO_2 occurs after the conventional combustion step. The CO_2 produced is separated from N_2, O_2, NOx, SOx and any other flue gases by adsorption, absorption or membrane separation [6]. This technology can be utilized directly in the existing power plants as an extension, thus saving the expense of construction of new plants. But the separation of CO_2 from flue gases requires significant energy input.

Fuels burned by *Oxyfuel* are burnt with oxygen in recycled flue gases instead of air [7]. In this case, CO_2 and steam are the main components in the flue gas. Steam can be easily removed by condensation and CO_2 is acquired without energy intensive gas separation. Instead of CO_2 separation, O_2 is separated from nitrogen in the air. This separation requires large amount of energy.

The technologies mentioned above all involved gas separation processes with intensive energy consumption and high cost for separation units. Chemical-looping combustion (CLC), which is the main topic of this thesis, involves no gas separation step, yet CO_2 is obtained in almost pure form after simple condensation of steam, meaning that there are no energy losses for the separation step and no equipment needed to perform the gas separation. Chemical-looping thus provides a possible, more economically feasible route for CCS compared to the alternatives above.

1.1.1 Chemical-looping combustion and Chemical-looping with oxygen uncoupling

Chemical-looping combustion is an innovative combustion technology in which there is no direct contact between combustion air and fuel. A CLC unit consists of two reactors, an air reactor and a fuel reactor, see Figure 1 [8].

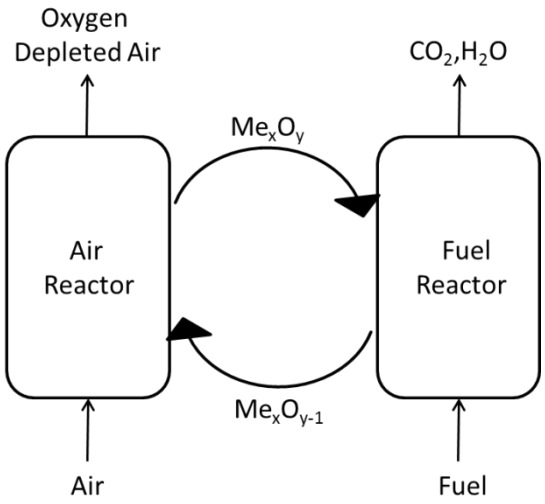

Figure 1. Schematic representation of the CLC process.

Solid oxygen carriers, which are usually metal oxide particles, are oxidized in the air reactor according to reaction 1 and circulated to the fuel reactor, where they are reduced by the fuel according to reaction 2. The oxygen needed for fuel conversion is supplied by the solid oxygen carrier particles. The reduced particles are recirculated to the air reactor and the process is repeated. The heat produced by CLC is the same as in conventional combustion which is seen by combining reaction 1 and 2. After steam condensation, high purity CO_2 ready for compression and storage is obtained after the fuel reactor. By transferring oxygen by solid oxygen carriers, the combustion products are not diluted with N_2 from the air. Thus the energy required for gas separation is avoided. Also, the CO_2 capture efficiency in CLC can reach 100% [9, 10]. These unique features make the CLC process a very interesting option for CO_2 capture.

$$O_2 + 2Me_xO_{y-1} \rightarrow 2Me_xO_y \quad (1)$$

$$C_nH_{2m} + (2n + m)\ Me_xO_y \rightarrow nCO_2 + mH_2O + (2n + m)\ Me_xO_{y-1} \quad (2)$$

In the fuel reactor, certain kinds of oxygen-carrier materials are able to release gaseous oxygen according to reaction 3. In a subsequent step, the fuel reacts directly with the released oxygen according to reaction 4. Such a process is referred to as chemical-looping with oxygen uncoupling (CLOU) [11].

$$2Me_xO_y \rightarrow 2Me_xO_{y-1} + O_2 \quad (3)$$

$$C_nH_{2m} + (n + 1/2m)\ O_2 \rightarrow nCO_2 + mH_2O \quad (4)$$

Oxygen carriers with the ability to release gas phase O_2 are referred to as CLOU materials. Here the oxygen released can react directly with the fuel through normal combustion, hence completely altering the fuel conversion mechanism. Depending upon the release rate of oxygen, this could be more favorable for the combustion process compared to conventional CLC: This is especially true for solid fuels, where the char can react directly with the released gaseous oxygen, thus avoiding the slow gasification step, and the reaction rate can be greatly enhanced [11]. For conversion of petroleum coke, it was reported that the reaction rate was about 45 times higher in the presence of Cu-based CLOU materials compared with a normal Fe-based CLC oxygen carrier [12, 13]. CLOU may have advantages with respect to gaseous and liquid fuel combustion as well. The gas phase oxygen could compensate for bad mixing in the fluidized bed and also the oxygen could convert fuel in the freeboard above the bed, thus enhancing the overall combustion efficiency. Materials with oxygen uncoupling properties are thus favored for both gaseous, liquid and solid fuel combustion [14].

1.2 Oxygen carriers

Oxygen carriers are metal oxides which can be cyclically oxidized and reduced when exposed to different conditions. For a metal oxide to be an oxygen carrier applied to the CLC process, certain properties of a material are required:

a) Suitable thermodynamic and kinetic properties under combustion conditions.
b) The performance should be stable in long time operation.
c) Good fluidizing properties, e.g. the particles should not form agglomerations.
d) The particles should have resistance against attrition and high mechanical strength.
e) The oxygen carrier should be environmental friendly and have reasonable costs.

Most oxygen carriers are based on the oxides of the transition metals, i.e. Ni, Fe, Mn and Cu. Some other materials, such as Al_2O_3 and ZrO_2, are sometimes mixed with the active metal oxide, thus acting as a support material. The properties of the oxygen carrier, for instance hardness, stability and reactivity, can be improved by using support materials [15-17]. These types of support materials can be inert or active. An inert support does not react with the metal oxide, nor does it take part in the redox chemical reactions in the CLC system. On the other hand, an active support material is involves in chemical reactions, either by reacting with the active metal

oxide or taking part in the oxygen transfer process [18, 19]. Examples of support materials which have been studied in CLC are TiO_2, Al_2O_3, CeO_2, ZrO_2 and $MgAl_2O_4$ [20-23].

Different methods can be utilized to manufacture oxygen carriers, for instance mechanical mixing, wet impregnation, freeze-granulation, extrusion and spray-dying [24-28]. The manufacture process generally consists of mixing and homogenization of raw materials, production of particles and calcination of formed particles. The major differences in these techniques are how the particles are produced. Detailed information of manufacture methods can be found in the literature [24-28].

1.2.1 Monometallic metal oxides

The chemical and physical properties of oxygen carriers are vital factors for a CLC process. How much oxygen can be transferred by a redox reaction, namely the oxygen transfer capacity of the oxygen carrier, and the rate of reactions in the air and fuel reactor are directly related to the solid inventory and the rate of solid recirculation between the two reactors [9]. To best utilize the heating value of fuels, high conversion of fuels to CO_2 and steam in the fuel reactor is the target. Jerndal et al. did a comprehensive thermal analysis of metal oxide systems, where Co, Fe, Ni, Mn and Cu oxides were recommended as potential oxygen carrier materials for CLC [29].

CoO on different support materials were previously examined by different groups of researchers [30-35]. The general problems with utilization of CoO as oxygen carrier material are poor thermodynamics for fuel (CH_4, CO and H_2) conversion, high cost and toxicity. Fe-based oxides, on the other hand, are cheap and environmentally friendly and have attracted great attention for use as oxygen carrier material, both with and without support material [36-45]. Disadvantages with Fe-oxides could be the low oxygen transfer capacity and CH_4 conversion achieved under CLC conditions [20, 46-48]. Also, iron oxide does not have appreciable CLOU property. But due to its abundance and low price, Fe oxide is still a potential oxygen carrier material.

NiO is the most studied oxygen carrier material due to its high reactivity and good performance [49]. It can be considered as the benchmark oxygen carrier for natural gas combustion. The influence of preparation method, effect of support material, amount of loading etc on the performance of the produced NiO oxygen carrier have been studied[16, 50-62]. Among a large number of studied oxygen carriers, two NiO-based oxygen carrier have been successfully demonstrated in 10 kW [63, 64] and 120 kW CLC units [65]. In the 10 kW unit at Chalmers University of Technology, a NiO based material has been operated for more than 1000 h achieving high CH_4 conversion and very low loss of fines, extrapolating to over 30 000 h of life time for the carrier [63]. However, NiO-based materials are expensive and toxic, and also suffer from thermodynamic restrictions for CH_4 conversion where about 1 vol% of partial oxidized products CO and H_2 exist in the flue gas [26, 51, 66]. For CLC application in the future, it may be difficult to use an expensive and toxic material like NiO. Other safer and cheaper oxygen carriers are needed to fulfill the economic and health requirements of a viable technology.

Another material which can be used as oxygen carrier is manganese oxide. Mn-oxides have the advantage of relatively low cost and are not burdened with major environmental issues like NiO. For Mn-oxides, full conversion of CH_4 to CO_2 and H_2O is thermodynamic favored. Also, the oxygen transfer capacity is higher for Mn oxide compared to Fe-oxide materials [29]. Moreover, Mn_2O_3 is capable of releasing oxygen in inert atmosphere which means that it has CLOU properties. But the oxidation of Mn_3O_4 to Mn_2O_3 is thermodynamically hindered at temperatures above ≈800°C [67]. At lower temperatures, where there are no thermodynamic limitations, the oxidation of Mn_3O_4 to Mn_2O_3 is still hard to achieve, probably due to kinetic limitations [67]. One method to change the behavior of Mn-based metal oxides is to incorporate other metals. These, so-called combined oxides is a major focus of this thesis and will be discussed further below.

Table 1. *Calculated equilibrium volume fraction of O2 at P_{tot}=1 atm over CuO/Cu_2O for reaction (5) as function of temperature.*

Temperature *(°C)*	**Equilibri. vol. fraction** *(vol%)*	**P_{O2}** *(atm)*
800	0.1	0.001
825	0.2	0.002
850	0.4	0.004
875	0.8	0.008
900	1.4	0.014
925	2.4	0.024
950	4.2	0.042
975	7.0	0.07
1000	11.4	0.114

Another alternative to NiO could be CuO-based materials. CuO is a CLOU material, and can decompose to Cu_2O when the surrounding oxygen partial pressure is below the CuO/Cu_2O equilibrium partial pressure at the reaction temperature. According to reaction 5, the amount of oxygen released can be up to 10 wt% of the fully oxidized CuO. The concentration of the O_2 released is related to the equilibrium oxygen partial pressure of CuO/Cu_2O which is a function of temperature, see Table 1. Further reduction of Cu_2O to Cu requires the presence of reducing agents but the formation of Cu is not preferred. This is because metallic Cu has a comparably low melting temperature (1085°C), and thus there is a high risk for agglomeration and defluidization problems at temperatures of relevance for combustion.

$$2CuO(s) \rightarrow Cu_2O(s) + ½O_2(g) \qquad (5)$$

Many studies have been done on CuO-based materials due to its pronounced CLOU property, high oxygen transfer capacity and high reactivity towards fuels [15, 21, 25, 68-74]. Support material Al_2O_3, ZrO_2, $MgAl_2O_4$, TiO_2 and SiO_2 with CuO have been examined by several research groups. It was found that some CuO-based materials started to agglomerate and defluidize at moderate temperatures [39, 75, 76] or reacted with the Al_2O_3 support losing parts of the CLOU ability [77]. Further development of CuO materials, which are resistant towards

agglomeration and stable in performance, is a requirement for further application within CLC/CLOU. In Paper VII, the performance of CuO on some inert and semi-inert support materials was investigated.

1.2.2 Combined metal oxides

To overcome the disadvantages of the monometallic oxygen carrier, one idea is to combine metal elements to form combined metal oxide system [27, 67, 78-82]. As discussed above, manganese oxides have oxygen uncoupling properties, but the relevant partial pressures of oxygen for CLOU reactions require rather low combustion temperatures in order to utilize the CLOU effect. However, several works have shown that Mn in combination with some other metals/metalloids can have significant advantages and also alter the thermodynamics in a positive way. The combined Mn-oxides are designed to have better thermodynamic and kinetic properties compared with pure Mn oxides, which means good redox property, CLOU property and high CH_4 conversion [83].

Elements such as Fe, Cu, Mg and Si are possible to combine with manganese oxides to form combined oxides [27, 28, 78, 84-87]. The $(Mn_yFe_{1-y})O_x$ system was examined and reported to be able to release gaseous O_2 and showed high reactivity towards methane and wood char without re-oxidation difficulty [28, 40, 84-88]. Oxygen carriers in the $(Mn_yCu_{1-y})O_x$ system achieved over 90% CH_4 conversion in a batch fluidized bed reactor. The uncoupling properties of oxygen were substantial, with 2% oxygen measured in the gas phase at 950°C when the particles were fluidized with an inert gas [27].

The calcium manganite $CaMnO_{3-\delta}$, which can be thought of as a combined oxide of Ca and Mn, has attracted attention for use in chemical-looping [89-93]. This type of materials has a defect perovskite structure with the general formula $ABO_{3-\delta}$. In such a structure, the oxygen deficiency δ may vary depending on the surrounding oxygen partial pressure or temperature as [94, 95]. When the surrounding oxygen partial pressure decreases, the defect grows by releasing oxygen according to reaction 6, and this oxygen can be utilized by the fuel in accordance with the CLOU process described above.

$$2ABO_{3-\delta} \rightarrow 2ABO_{3-\delta-a} + aO_2 \qquad (6)$$

One promising feature of such materials is that there is no distinct phase transition between oxidized $ABO_{3-\delta}$ and reduced $ABO_{3-\delta-a}$. This may be advantageous and may help in avoiding the problem caused by structural changes between oxidized and reduced phase. $CaMn_{0.875}Ti_{0.125}O_3$ has been examined in TGA, batch fluidized reactors and small scale continuous fluidized bed reactors, showing good CLOU properties, high reactivity towards methane and good fluidization behavior [90, 91]. In this work, a major effort was devoted to development of this type of material. In Paper I and II, a general screening of calcium manganite with different additives was performed. Based on the screening results, the influence of operation temperature and production parameters on the performance of selected calcium manganite oxygen carriers were examined in Paper III and IV. Further, to enable up-scaling

production to the industrial level, raw materials available in tonnage scale were screened and used for the calcium manganite oxygen carrier manufacture using spray-drying method. The properties of the calcium manganite produced from commercially available raw materials were examined in Paper V.

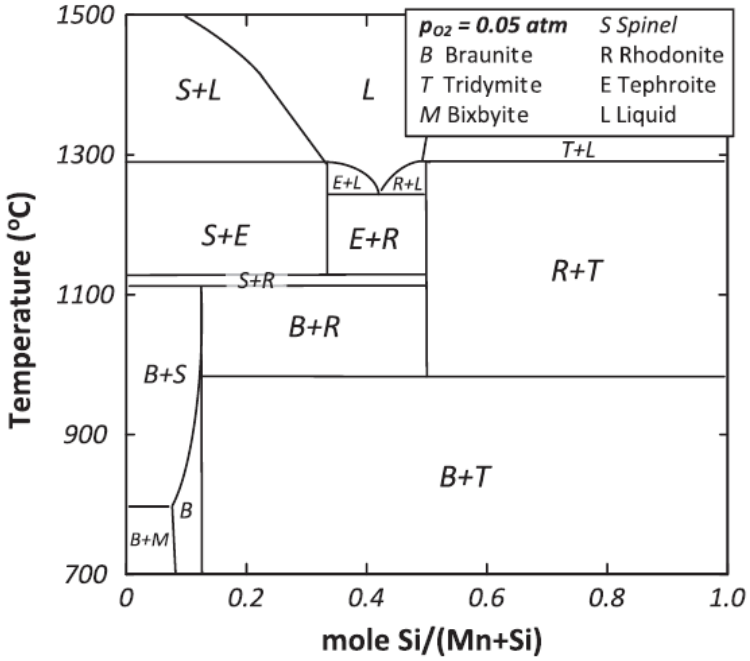

Figure 2. Phase diagram of Mn-Si binary oxide system where the O_2 partial pressure is 0.05 atm [96]**.**

Another interesting combined manganese oxide is the combination of Mn with Si. Manganese silicate oxides, such as braunite Mn_7SiO_{12}, rhodonite $MnSiO_3$ and tephroite Mn_2SiO_4, are products of the combination of Si and Mn at different Si/Mn ratios. Figure 2 is a calculated phase diagram of this binary system where the oxygen partial pressure is 0.05 atm [96]. Together with single oxide phases, spinel Mn_3O_4, tridymite SiO_2 and bixbylite Mn_2O_3, the phase diagram suggests different phase transitions among these Mn-Si oxides. These transitions are reversible and gaseous oxygen is provided when the Mn oxidation state decreases. For instance, for a Si/(Mn+Si) molar ratio of 0.4, when the temperature increases to around 1000°C, braunite Mn_7SiO_{12} reacts with tridymite SiO_2 forming rhodonite $MnSiO_3$ and O_2 is produced, see reaction 7. A comprehensive study of Mn-Si oxide system is presented in Paper VI.

$$(2/3)Mn_7SiO_{12} + 4SiO_2 \rightarrow (14/3)MnSiO_3 + O_2 \quad (7)$$

The combination of Mg with Mn can form a solid solution $(Mg_{1-x}Mn_x)O$ and $(Mg_xMn_{3-x})O_4$ or compounds Mg_6MnO_8, Mg_2MnO_4, $MgMn_2O_4$ below 1000°C depending on the Mg/Mn ratio [97]. These solutions and compounds are not stable during variation of oxygen partial pressure and temperature. Certain transformations can occur between these structures together with releasing

or uptake of oxygen [96, 97], which make them possible CLOU oxygen carriers. Suggested transformation reactions are [96]:

$$Mg_2MnO_4 \rightarrow [1-(1/(1+x))]\ (Mg_{2-x}Mn_{1+x})O_4 + [1+x]\ MgO + [1/(1+x)]\ O_2 \quad (8)$$

$$4Mg_2MnO_4 \rightarrow 2MgMn_2O_4 + 6MgO + O_2 \quad (9)$$

$$6MgMn_2O_4 \rightarrow 4Mn_3O_4 + 6MgO + O_2 \quad (10)$$

Prior to the work in this thesis, the $(Mn_yMg_{1-y})O_x$ and $(Mn_ySi_{1-y})O_x$ system has been briefly investigated as potential candidate for CLC and CLOU applications [78, 87, 98]. In this work, an extensive study was conducted for the Mn-Si system. Further, several Mn-Mg materials have been investigated, and the results are presented in Paper I. Here, a number of different binary and ternary systems are explored based on Mn with Fe, Mg, Si and Ca.

1.3 Objective

The aim of this thesis is to screen and investigate viable oxygen carriers for CLC and CLOU which do not contain nickel and have the potential to replace the benchmark Ni-based material. This will likely have advantages with respect to oxygen carrier cost as well as health and environmental benefits. As it is likely that oxygen carriers which have oxygen uncoupling properties have advantages with respect to fuel conversion rates, the focus has been on finding materials which release all or some of their available oxygen as gas-phase O_2. The research has been focused on the perovskite $CaMnO_{3-\delta}$, as well as on Mn-Si and Mn-Mg oxide systems. The main focus is on utilization of CH_4, which is the main component in both natural gas and refinery gas, as fuel. In addition, some work has been done on CuO based materials with focus on the reactions important for CLOU. The main results of the screening work are presented in this thesis, and the details of the work can be found in the appended papers.

2 Experimental

2.1 Manufacture and characterization of oxygen carriers

2.1.1 Oxygen carrier manufacture method: spray drying

The production of oxygen carriers was conducted by VITO (Flemish Institute for Technological Research) using a spray-drying method. This industrial process can produce highly spherical, free-flowing, micro scale homogeneous oxygen-carrier particles. Inorganic raw materials were weighed and dispersed in deionized water with organic binders and dispersants. The water based suspension was then ball-milled for homogenization. In Paper IV, the milling time was set to 5 min, 15 min or 45 min individually to study the effect of milling. In the rest of attached publications, the milling time is set to 5 min if not specified. After milling, the spray dry suspension is transferred to a container and a propeller blade mixer is used to stir the homogenized slurry while it is being pumped into an atomizer located in the drying chamber. The injected slurry first form droplets due to the effect of surface tension. The droplets are dried during the time of flight by heated air and then become dry particles that are separated from the hot air. The spray dried particles were sieved before calcination.

Calcination was conducted in natural convection furnaces (Entech, Sweden and Bouvier, Belgium) under an air atmosphere. Here the spray-dried particles were placed in an alumina crucible. Sieved particles were heated from room temperature to the desired temperature, i.e. calcination temperature, and were kept for a certain period of time to facilitate possible chemical reactions and obtain sufficient mechanical strength [47]. Then the oven was cooled down to room temperature in air. Calcined particles with diameter 125-180 μm were obtained by sieving for bulk density measurement and reactivity test, and 180-212 μm particles were used for crushing strength measurement. Detailed information about the synthesis composition, milling time, calcination temperature and calcination time of the examined oxygen carriers can be found in the attached papers.

2.1.2 Oxygen-carriers manufactured

A significant number of material compositions were investigated in this work. Calcium manganese based materials were investigated in Paper II, six materials with addition of either Ti, Fe or Mg. Two of these were further examined in Paper III. Another 17 related materials were examined in Paper V, all having the general formula $CaMn_{0.775}Mg_{0.1}Ti_{0.125}O_{3-\delta}$. These materials used different sources of raw materials, thus having different compositions due to the impurities. Eleven different compositions of manganese silicate materials were examined in Paper VI. Moreover, binary and ternary manganese systems were examined in Paper I, including Mn-Mg, Mn-Fe-Ca, Mn-Ca-Mg, Mn-Fe-Mg and Mn-Fe-Si, totally 16 materials. Lastly, twelve copper-based materials were studied in Paper VII. Thus, 62 different material compositions were examined. The total number of materials investigated, however, was significantly larger as many of these compositions were sintered at different temperatures. Moreover, the effect of production parameters are studied in Paper IV, where 15 calcium

manganite materials with the same composition, but with different milling time, calcination time and calcination temperature are compared.

2.1.3 Techniques used for oxygen carrier characterization

The bulk density of the oxygen carriers produced was calculated by using the mass of fresh particles with diameter 125-180 µm divided by its volume which was measured using a graduated cylinder. The mechanical strength of the sample referred to as crushing strength (CS) was measured on fresh particles with a diameter of 180-212 µm by a digital apparatus (Shimpo FNG-5). XRD utilizing Cu Kα1 radiation (D5000 Advanced, Siemens and D8 Advanced, Bruker AXS) and BET (ASAP2000, Micromeritics and TriStar 3000, Micromeritics) was employed to study the chemical composition, crystalline structures and the specific surface area of the material. The porous nature of selected oxygen carriers were measured on a few materials using a mercury intrusion (Poremaster, Quantachrome) method. The morphology and surface elements composition of the oxygen carrier was studied by SEM/EDX microscope (TM3030, Hitachi and Quanta 200 Environmental, FEI). Light microscopy were also used to provide morphology information of the studied materials.

The resistance to mechanical attrition of the different samples was examined using a lab scale attrition rig. A used sample from the reactivity test with a mass of 5 g was placed in a conical cup which is located at the bottom of a gravitational separator. The jet cup consists of a 39 mm high conical cup with an inner diameter of 13 mm in the bottom and 25 mm in the top. A nozzle with an inner diameter of 1.5 mm is located at the bottom of the cup, and tangentially in relation to the cup wall. During operation, air is added with a velocity of approximately 100 m/s through the inlet nozzle, creating a vortex of particles swirling upwards through the cup. The gravitational separator has a height of 634 mm and an inner diameter of 216 mm. At the top of the separator, a filter (Parker P31FA12CGMN) was mounted in which fine particles were collected. The filter was dismantled every 10 min and was weighed to measure how much fines were produced. The apparatus was operated at room temperature and roughly atmospheric pressure. After 1 h test, an attrition index of a material was calculated based on the results obtained during the last 30 min, see section 2.3.2 for the calculation of attrition index. A detailed description of the test rig and methodology can be found in literature [99].

2.2 Experimental setup and procedure

2.2.1 Batch fluidized bed system

The reactivity tests were conducted in a batch fluidized bed system, see Figure 3. An 870 mm long quartz reactor with the inner diameter of 22 mm was used as the reaction chamber to simulate the continuous chemical-looping combustion conditions. A certain amount of particles were placed on a porous plate located at 370 mm above the bottom of the quartz reactor. Temperature was measured 25 mm above and 5 mm underneath the porous plate by Pentronic

CrAl/NiAl thermocouples inside quartz shells. The pressure drop over the reactor was recorded by Honeywell pressure transducers with a frequency of 20 Hz.

Oxygen carrier particles with diameter 125-180 µm were weighed and placed on the porous plate before introducing gases from the bottom of the reactor. Flue gases exiting from the top of the reactor were cooled by an electric cooler for steam condensation. The cooled gases were sent to the Rosemount NGA-2000 gas analyzer where the concentrations of CO, CO_2, CH_4 and O_2, together with the flow of the dry gas were quantified.

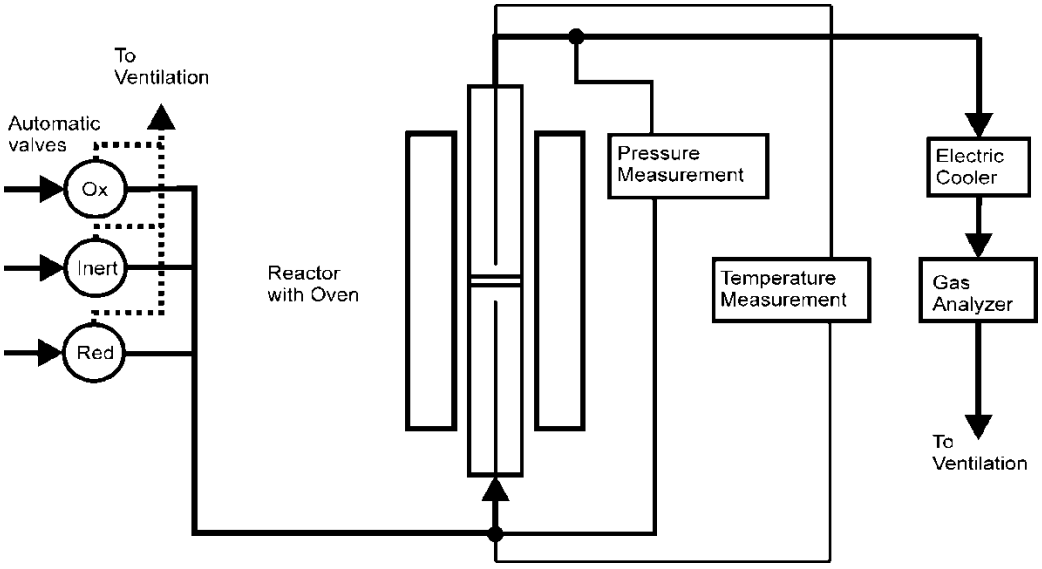

Figure 3. Schematic representation of laboratory set-up of a batch fluidized bed system.

2.2.2 Experimental scheme

The exact experimental conditions applied in this thesis varied depending upon the type of test and oxygen carrier material. In general, a mass of 15 g oxygen carrier particles was exposed to oxidation (5% O_2 in N_2) and inert/reduction environments (100% N_2/CH_4 or syngas) alternatively to simulate the circulating conditions in a continuous CLC system. The CLOU properties of the oxygen carrier, or the ability to release oxygen to the gas phase, were examined by measuring the oxygen concentration in the outlet stream during 360 s where the particles were fluidized with N_2. The reactivity tests towards fuels were carried out by injecting CH_4 or syngas (50% CO and 50% H_2) for 20 s or 80 s. Before and after each fuel injection, 100% N_2 was used to flush the reactor for 60 s preventing back-mixing of remaining fuels or inlet oxygen. The applied gas flows were 900 mL_N/min for 5% O_2 (in N_2), 600 mL_N/min for N_2 and 450 mL_N/min for CH_4 and syngas. The reactivity tests were carried out at 850-1100ºC based on the specific aim of the test and the property of the oxygen carrier. In Paper III, when investigated the reactivity stability and the influence of reduction time on the oxygen carrier, the bed mass was reduced to 2 g and 10% O_2 was used as an oxidation environment instead of 5% O_2. The gas flow was set to 900 mL/min for all gases, i.e. 10% O_2, 100% N_2 and CH_4. This was done to

shorten the time for oxidation and reduction, so more cycles can be performed. For a more detailed description of the type of experiments made in this work, see attached papers.

2.3 Data evaluation

2.3.1 Methane conversion and solid conversion

Fuel conversion, or fuel yield γ, is defined as the degree of how much introduced fuel has been fully converted into CO_2. It is used to quantify an oxygen carrier's reactivity towards fuels. Methane conversion is calculated using equation 11 and equation 12 shows the CO conversion. Although the syngas contains a mixture of CO and H_2, hydrogen was not measured during the experiments, and thus the syngas conversion is simply presented by the CO conversion.

$$\gamma_{CH4} = \frac{p_{CO_2}}{p_{CO_2} + p_{CO} + p_{CH4}} \tag{11}$$

$$\gamma_{syn} = \frac{p_{CO_2}}{p_{CO_2} + p_{CO}} \tag{12}$$

where p_i is the outlet partial pressure of component i. A fuel yield of 1 corresponds to full conversion of the fuel.

Oxygen carrier conversion, or solid conversion ω, is defined as:

$$\omega_i = \frac{m_i}{m_{ox}} \tag{13}$$

where m_i is the mass of the oxygen carrier at time i and m_{ox} is the mass of the fully oxidized oxygen carrier. In a fuel reduction period, ω can be calculated as a function of time. Equation 14 and 15 are used to calculate the oxygen carrier conversion during a methane and syngas reduction period respectively:

$$\omega_i = \omega_{i-1} - \int_{t_{i-1}}^{t_i} \frac{\dot{n}_{out} M_o}{m_{ox} P_{tot}} (4p_{CO_2,out} + 3p_{CO,out} + 2p_{O_2,out} - p_{H_2,out}) dt \tag{14}$$

$$\omega_i = \omega_{i-1} - \int_{t_{i-1}}^{t_i} \frac{\dot{n}_{out} M_o}{m_{ox} P_{tot}} (2p_{CO_2,out} + p_{CO,out} + 2p_{O_2,out} - p_{H_2,out}) dt \tag{15}$$

Here, $\dot{n}_{out}$ is the molar flux of flue gas after water condensation, M_o is the molar mass of oxygen, and P_{tot} is the total pressure of the outlet gas. For a specific reduction cycle, the fuel conversion is often given as an average value corresponding to the conversion yield in the

interval of ω =1 to 0.99 or over the entire reduction period (when ω does not decrease to 0.99 if the material is not very reactive). The concentration of H_2 was not measured during the experiments. It can be assumed to be low enough to be neglected since H_2 generally has a higher reactivity than CO [100] and the CO concentration was very low under all conditions.

2.3.2 Attrition index

The resistance to mechanical attrition of oxygen carrier materials was examined in a lab scale attrition rig and indicated by the attrition index. A mass of 5 g particles collected after reactivity testing was selected for the 1 h attrition test. Every 10 min, the filter at the top was dismounted and weighed to measure the mass of fines produced.

The accumulated attrition is derived from the mass of fines produced over the mass of original sample, i.e. 5 g. Experimental data of the last 30 min (symbols) as a function of time is presented in Fig. 4 where an attrition index A_i is calculated. Solid lines in the figure are linear fits of experimental data, and the slope of the fits is taken as the attrition index A_i.

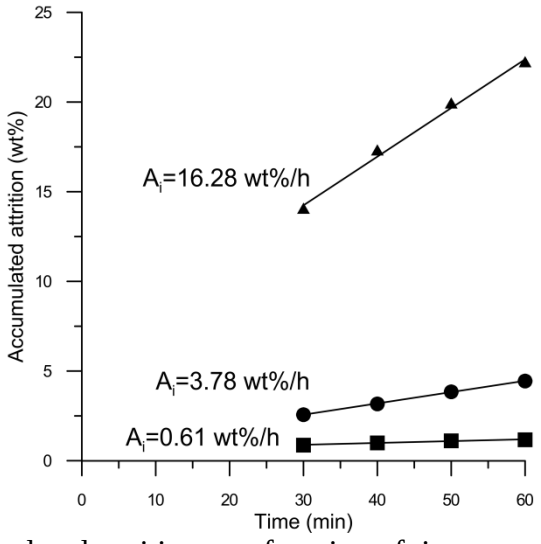

Figure 4. The accumulated attrition as a function of time.

3 Results

In this thesis, a series of oxygen carrier materials were prepared by spray-drying and investigated with respect to parameters important for CLOU. The materials are based on *i)* combined Mn-oxides and *ii)* Cu-based materials. As outlined previously, both of these type of systems may have the propensity to release oxygen to the gas phase in combustion conditions. In paper I, several binary and ternary Mn-systems were investigated based on combinations of Mn with one or two metals/metalloids: Fe, Mg, Ca and Si. The general conclusion from this study was that the binary systems had better reactivity with methane, with the most interesting systems based on Mn-Ca, Mn-Si and Mn-Mg. The ternary system of most interest was the Mn-Fe-Si. Below the focus will be on the promising system Mn-Ca, Mn-Si and Mn-Mg. The oxygen carriers can be categorized with respect to the active system, see Table 2-5 below.

Perovskite type $CaMn_{0.875}Ti_{0.125}O_3$ has been previously studied and exhibited promising behavior [89-91]. Despite the interest in this kind of material, a systematic study on perovskite type calcium manganite was missing in the literature before the initiation of this work. Hence, the behavior of seven perovskite structured calcium manganite with Fe, Ti and Mg addition were investigated with respect to parameters important for CLOU, i.e. release behavior of oxygen and reactivity towards gaseous fuels, primarily methane. When Mg and/or Ti were added, the calcium manganite showed the best results among the investigated oxygen carriers. In recent years, after the screen study performed in this thesis, calcium manganite with Mg and/or Ti additives has attracted great interest and has been tested in lab scale continuous CLC units where promising results have been achieved [93, 101-103]. Almost all the examined calcium manganite were produced by spray drying method. However, there is no research on the influence of basic production parameters, such as calcination time, calcination temperature and milling time, on the property of spray dried $CaMnO_3$ prior to the study presented in Paper IV. Moreover, for CLC to be applied at an industrial level, tonnage scale production of oxygen carriers are required. This requires not only cheap raw materials, but they must also be available at sufficient scale. Certainly, cheap raw powders may be less pure, which may affect the behaviour of the final material. Paper V presents an extensive investigation of the most promising calcium manganite with a molar composition of $CaMn_{0.775}Mg_{0.1}Ti_{0.125}O_3$. This composition was produced using different sources of Mn and Ti, all of which are readily available at tonnage scale, and the resulting materials were compared.

Another interesting combined oxide system, which had not been widely investigated, was the Mn-Si-O system [87, 98]. A thermodynamic analysis by Rydén et al. suggests that it has the potential to be utilized for CLOU [96]. In this thesis, fifteen Mn-Si-O oxygen carrier materials with different Si/(Si+Mn) molar ratios were produced and investigated. The Si/(Mn+Si) molar ratios were between 3% and 79% which covered most of the interesting areas in the phase diagram, see Figure 2. The Mn-Mg-O materials examined in this work had molar ratio of Mn/Mg equal to 2, 1.5 and 1 respectively, and is an extension of the work performed by Shulman et al. [78].

Table 5 contains the Cu-based oxygen carriers produced. As was discussed above, there had been development of this system prior to the work in this thesis, e.g. CuO/Al_2O_3, CuO/ZrO_2,

$CuO/MgAl_2O_4$ had been investigated [25, 39, 70, 71, 104]. However, some of the investigated CuO oxygen carriers suffered from agglomeration or high attrition problems [25, 71]. On the other hand, some other support materials, for instance CeO_2 and stabilized ZrO_2, had not yet been examined as support for CuO. In this work, support materials based on CeO_2 and stabilized ZrO_2 were investigated in order to establish if high reactivity and better stability could be obtained compared to earlier tested supports. In addition, two different types of $MgAl_2O_4$ were used as support in order to examine if the actual raw material used during production could have an effect on oxygen carrier's behavior. Finally, some CuO samples were produced employing Fe_2O_3 with or without Mg or Mn addition, with the aim of producing active or non-active mixed oxides.

3.1 Physical properties

The hardness of the particles can be measured by crushing strength, and a crushing strength of minimum 1 N is a practical criterion when selecting oxygen carriers. If an oxygen carrier had a crushing strength of less than 1 N, it was regarded as prone to break apart and be blown out of the reactor, and hence not deemed appropriate to test in this work. Nevertheless, for some materials, soft samples were still examined in the fluidized bed, if particles with higher crushing strength were not available for a given composition. However, it should be noted that Rydén et al. found that a crushing strength of above 2 N may be needed in order to achieve sufficient resistance towards attrition [99]. Detailed information of crushing strength and bulk density can be found in the following tables.

In Table 2-5, oxygen-carrier notations were given based on raw materials. Letters represent the raw oxide materials, which can be summarized as: C=$Ca(OH)_2$, M=Mn_3O_4, F=Fe_2O_3, T=TiO_2, Mg=MgO, Si=SiO_2, Cu=CuO, Zr=ZrO_2, La=La_2O_3, YSZ=Y_2O_3 stabilized ZrO_2, Ce=CeO_2, MgAl=$MgAl_2O_4$. $MgAl^x$ in Table 5 is a finer and more expensive $MgAl_2O_4$ than the one used for the MgAl sample. The Arabic number after the letters shows the weight percentage of the raw material used in the synthesis recipe, i.e. the water-based slurry which was spray-dried.

It is clear from the tables that materials with a wide range of bulk densities and crushing strengths were obtained in this work. For the Mn-Si materials, low crushing strengths were obtained, see Table 3, independent of the calcination temperature and composition. It is likely that some type of optimization would be needed to increase the material strength to a reasonable level, although some of the materials actually displayed a reasonably low resistance to attrition, see Paper VI. This was not done as part of this work, however. For the calcium manganites shown in Table 2, a CS of above 1 N was found for the materials calcined at 1300ºC. It was found in Paper II that higher densities and strengths could be obtained using higher calcination temperatures. Further, milling time and calcination time are production parameters which could also be used to obtain more stable material, see below.

The impact of calcination temperature, calcination time and milling time on the physical properties of spray dried oxygen carrier was studied on C52MMg3 material. This composition is used in the C14 material, which has been investigated in several publications. Calcination

temperature for the spray dried particles varied from 1300ºC to 1350ºC, and the calcination time was 4 h, 8 h and 16 h respectively. As shown in Figure. 5, the bulk density and crushing strength of the studied oxygen carrier generally increased with calcination temperature and time, but decreased with milling time. For the material with low crushing strength, i.e. the one calcined at 1300ºC for 4h with a milling time of 5min, increase of milling time, calcination time or temperature had a positive effect on the crushing strength of the sample.

As seen in the figure, the BET surface area of all studied materials was quite low, i.e. below 0.4 m^2/g. However, the negative effect of high calcination temperature, long calcination time and milling time on the surface area can still be observed. The materials resistance against physical attrition correlates well with its bulk density and crushing strength as presented in Figure 6. Particles with higher bulk density/CS had a lower A_i value, which means less fines are expected to be produced during actual operation.

Table 2. *Summary of crushing strength and bulk density of Ca-Mn-X-O materials. All particles were sintered at 1300°C.*

Notation	**Molar Composition**	**Raw materials** (*wt%*)	**Bulk density** (*kg/m^3*)	**CS** (*N*)
C49MF5	$CaMn_{0.9}Fe_{0.1}O_{3-\delta}$	49.2 $Ca(OH)_2$, 45.5 Mn_3O_4, 5.3 Fe_2O_3	1552	1.4
C49MF11	$CaMn_{0.8}Fe_{0.2}O_{3-\delta}$	49.0 $Ca(OH)_2$, 40.4 Mn_3O_4, 10.6 Fe_2O_3	1680	1.4
C49MT3	$CaMn_{0.95}Ti_{0.05}O_{3-\delta}$	49.2 $Ca(OH)_2$, 48.1 Mn_3O_4, 2.6 TiO_2	1519	1.3
C49MT13	$CaMn_{0.75}Ti_{0.25}O_{3-\delta}$	49.0 $Ca(OH)_2$, 37.8 Mn_3O_4, 13.2 TiO_2	1433	1.3
C50MT7Mg3[a]	$CaMn_{0.775}Mg_{0.1}Ti_{0.125}O_{3-\delta}$	50.3 $Ca(OH)_2$, 40.1 Mn_3O_4, 2.7 MgO, 6.8 TiO_2	1343	1.4
C51MMg3[b]	$CaMn_{0.9}Mg_{0.1}O_{3-\delta}$	50.5 $Ca(OH)_2$, 46.8 Mn_3O_4, 2.7 MgO	1420	1.4
C52MMg6	$CaMn_{0.8}Mg_{0.2}O_{3-\delta}$	51.8 $Ca(OH)_2$, 42.6 Mn_3O_4, 5.6 MgO	1074	1.3

[a]also known as C28 when calcined at 1350ºC, [b]also known as C14

Table 3a. *Summary of crushing strength and bulk density of Mn-Si-O oxygen-carriers materials. Particles were sintered at 1050°C.*

Notation	**Si/(Si+Mn)** *(mol%)*	**Raw materials** (*wt%*)	**Bulk density** (*kg/m^3*)	**CS** (*N*)
MSi2	2.5	98 Mn_3O_4, 2 SiO_2	1091	0.5
MSi6	7.5	94 Mn_3O_4, 6 SiO_2	896	0.4
MSi10	12.4	90 Mn_3O_4, 10 SiO_2	1054	0.5
MSi15	18.3	85 Mn_3O_4, 15 SiO_2	1120	0.6
MSi20	24.1	80 Mn_3O_4, 20 SiO_2	990	0.3
MSi25	29.7	75 Mn_3O_4, 25 SiO_2	830	0.3
MSi30	35.2	70 Mn_3O_4, 30 SiO_2	806	0.4
MSi50	55.9	50 Mn_3O_4, 50 SiO_2	799	0.6

Table 3b. *Summary of crushing strength and bulk density of Mn-Si-O oxygen-carriers materials. Particles were sintered at 1150°C.*

Notation	**Si/(Si+Mn)** *(mol%)*	**Raw materials** (*wt%*)	**Bulk density** (*kg/m^3*)	**CS** (*N*)
MSi6	7.5	94 Mn_3O_4, 6 SiO_2	1250	0.3
MSi15	18.3	85 Mn_3O_4, 15 SiO_2	1200	0.5
MSi25	29.7	75 Mn_3O_4, 25 SiO_2	1210	0.5
MSi35	40.6	65 Mn_3O_4, 35 SiO_2	1000	0.5
MSi45	50.9	55 Mn_3O_4, 45 SiO_2	997	0.6
MSi50	55.9	50 Mn_3O_4, 50 SiO_2	884	0.4
MSi75	79.2	25 Mn_3O_4, 75 SiO_2	701	0.4

Table 4. *Summary of crushing strength and bulk density of Mn-Mg-O oxygen-carriers material.*

Notation	**Mn/Mg** *(mol%)*	**Raw materials** (*wt%*)	**Cal. temp.** *(°C)*	**Bulk density** *(kg/m^3)*	**CS** (*N*)
			1200	1318	2.5
MMg21	2	79.1 Mn_3O_4, 20.9 MgO	1300	1900	4.3
			1200	1454	2.5
MMg26	1.5	74.0 Mn_3O_4, 26.0 MgO	1300	1897	3.4
			1200	1385	1.4
MMg35	1	65.4 Mn_3O_4, 34.6 MgO	1300	1842	3.9

Table 5*.Summary of crushing strength and Bulk density of CuO-based materials.*

Notation	**Raw materials** *(wt%)*	**Cal. temp.** *(°C)*	**Bulk density** *(kg/m3)*	**CS** *(N)*
Cu40Z	40 CuO, 60 ZrO_2	950, 1100*	1950, 2270	3.4, 4.5
Cu40ZLa5	40 CuO, 55 ZrO_2, 5 La_2O_3	950, 1100*	1450, 1680	1.4, 1.3
Cu40(YSZ)	40 CuO, 60 YSZ	1000**, 1100	1480, 1700	0.4, 0.6
Cu40Ce	40 CuO, 60 CeO_2	950, 1100*	2170, 2820	1.0, 1.5
Cu40CeLa5	40 CuO, 55 CeO_2, 5 La_2O_3	950**, 1100*	2130, 2780	0.3, 1.3
Cu40(MgAl)	40 CuO, 60 $MgAl_2O_4$****	950**, 1100	1210, 1270	0.4, 0.9
Cu40($MgAl^x$)	40 CuO, 60 $MgAl_2O_4$****	950**, 1100	990, 1420	0.6, 1.4
Cu40(MgAl)La5	40 CuO, 60 $MgAl_2O_4$, 5 La_2O_3	950**, 1100	1200, 1180	0.4, 0.5
Cu60F	60 CuO, 40 Fe_2O_3	950, 1100***	2160, ***	1, ***
Cu40MF41	40 CuO, 41 Fe_2O_3, 19 Mn_3O_4	950*, 1100***	2100, ***	1.3, ***
Cu40MgF48	40 CuO, 48 Fe_2O_3, 12 MgO	950, 1100***	1810, ***	1, ***
Cu36FAl24	36 CuO, 40 Fe_2O_3, 24 Al_2O_3	950**, 1100	1090, 1870	0.4, 1.2

Note: * Defluidized during batch experiments, ** Very soft particles excluded from testing; *** Cake formation during calcination **** Cu40(MgAl) from two $MgAl_2O_4$ qualities, finer material with higher purity is marked “x”.

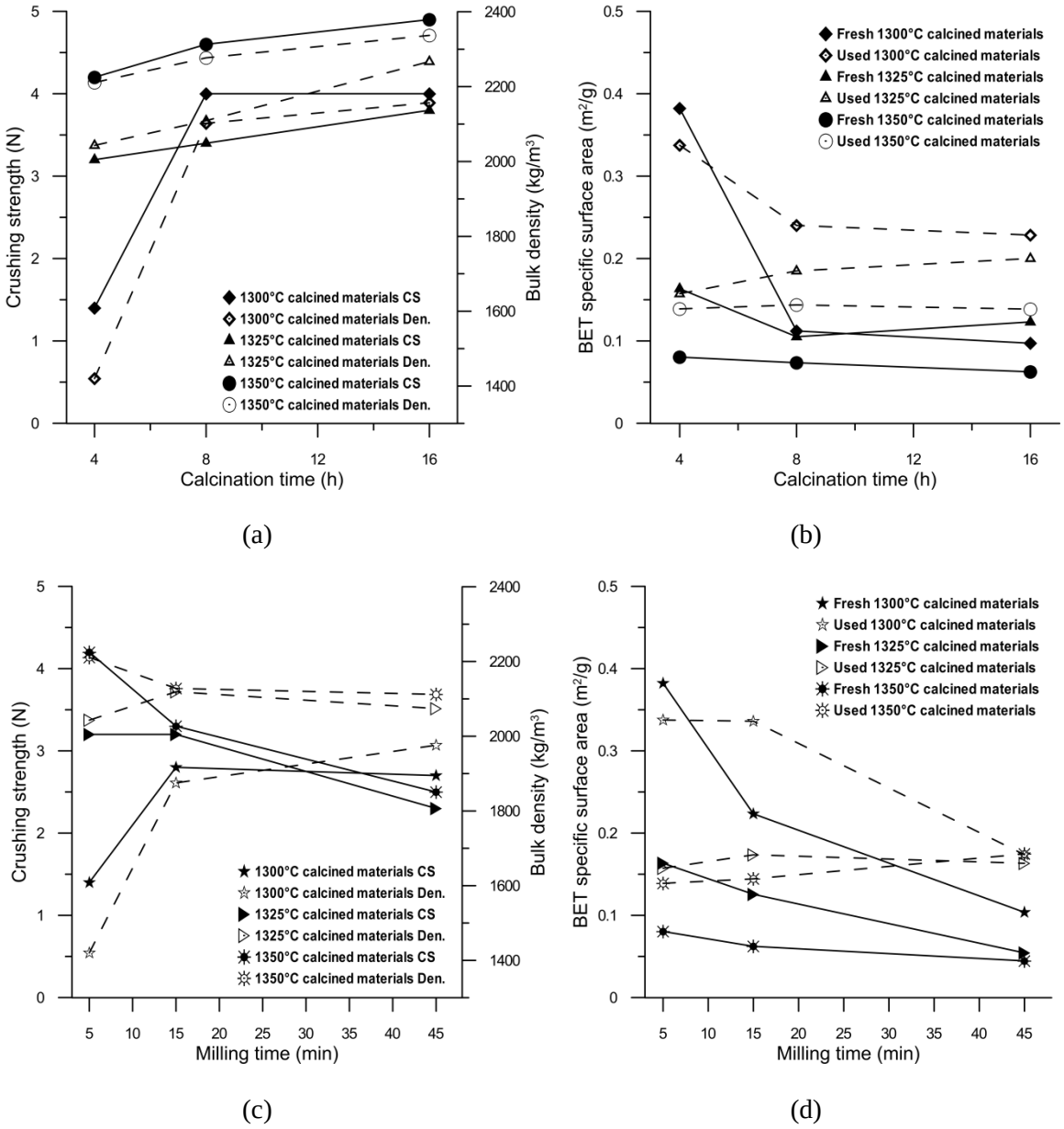

Figure 5. The crushing strength, bulk density and BET surface area as a function of (a) (b) calcination time and (c) (d) milling time. Oxygen carriers presented in 5a were milled for 5 min before spray drying. The calcination time for the oxygen carriers in 5b was 4 h. Continuous lines indicate crushing strength in (a) and (c), and fresh materials in (b) and (d).

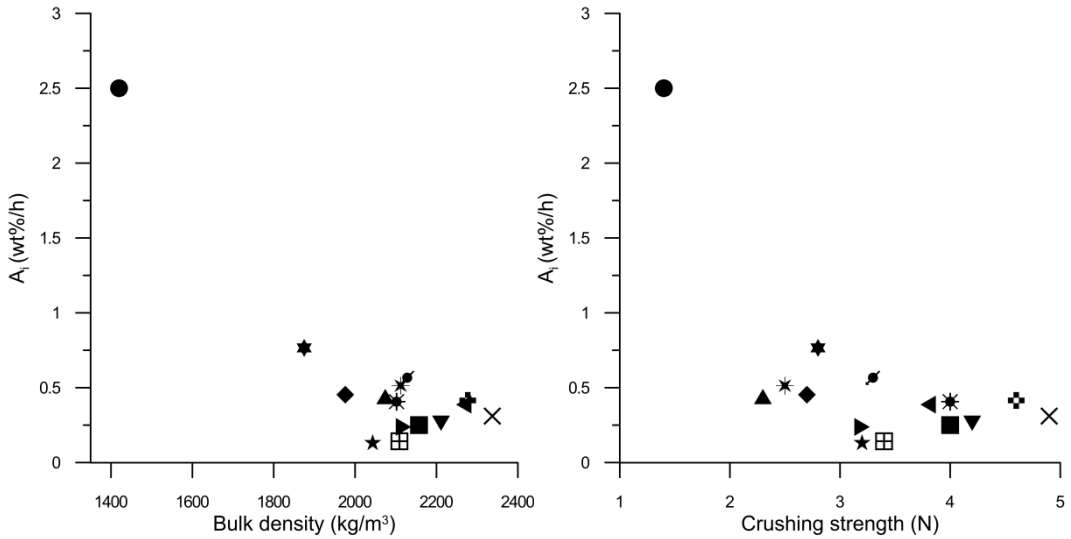

(a) (b)

Figure 6. The attrition index A_i as a function of (a) bulk density and (b) crushing strength for investigated C52MMg3 oxygen carriers.

●:1300C4h5m ✸:1300C4h15m ◆:1300C4h45m ✷:1300C8h5m ■:130016h5m
★:1325C4h5m ▶:1325C4h15m ▲:1325C4h45m ⊞:1325C8h5m ◀:1325C16h5m
▼:1350C4h5m ✐:1350C4h15m ✴:1350C4h45m ✜:1350C8h5m ✕:1350C16h5m

3.2 Oxygen uncoupling properties

Below follows some results from the experiments conducted to judge the oxygen uncoupling behaviour, or CLOU properties. In the thesis some of the general properties for the different systems will be illustrated, and the reader is referred to the attached papers for more information.

3.2.1 Combined manganese oxides

Combined manganese oxides could be of interest for chemical-looping with oxygen uncoupling (CLOU). As discussed above, oxidation of Mn_3O_4 to Mn_2O_3 is thermodynamically hindered at CLC operation temperature, i.e. 800°C or above.

By combining Mn with other elements, such as Ca, Fe, Mg and Si, the thermodynamics of oxidation reaction could be altered, which may also enable a release of oxygen at more relevant temperatures. In this thesis, some binary manganese oxides (Mn combined with one addition metal) and ternary manganese oxides (Mn with two additional metals) were investigated as oxygen carriers for chemical-looping with oxygen uncoupling (CLOU). Below follows a discussion on the uncoupling properties of the most interesting combined oxides.

3.2.1.1 Perovskite Ca-Mn-X-O (X=Fe, Ti and Mg) system

3.2.1.1.1 The effect of additives

The Ca-Mn-X-O (X= Fe, Ti and Mg) system investigated in this work includes seven perovskite structure materials with a general formula $CaMn_aX_{1-a}O_{3-\delta}$, see Table 2. The perovskite was identified by XRD in all fresh samples.

Figure 7 displays the O_2 concentration profile of the 2nd N_2 cycle at 900°C performed on these materials. At t=0 s, 100% N_2 was injected to the reactor system instead of 5% O_2. The concentration of oxygen in the outlet flow clearly decrease after the injection of N_2. Instead of dropping to 0 immediately, the measured oxygen concentration showed a sliding profile due to the oxygen uncoupling property (CLOU). The characteristic "sliding" profile is expected due to the oxygen deficiency given by 3-δ. At the end of the N_2 flushing cycle, the oxygen concentration remained at about 0.4 vol%. Thus, when combining Ca with Mn, together with some additive Ti, Fe and Mg, the formed perovskite calcium manganite presented CLOU behavior under CLC condition. Also, undoped perovskite will show similar behavior, but will likely have a large propensity to decompose. For materials made from combination of the same metal elements, i.e. Ca-Mn with Fe or Mg, but with a composition where Ca/(Mn+X) was not equal to unity, no CLOU property was discovered, see Paper I for detail information.

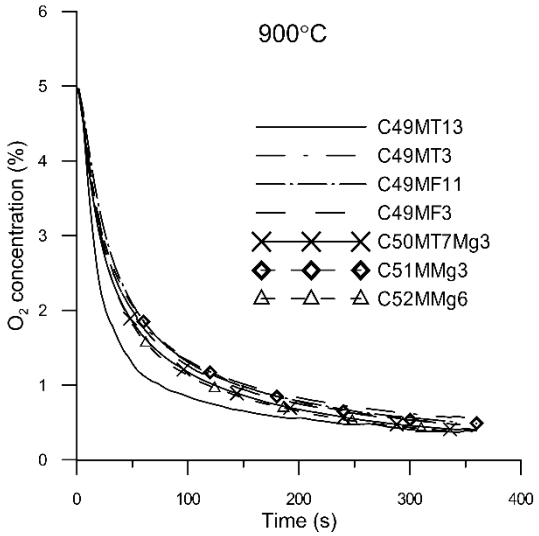

Figure 7. The O_2 concentration profile of the 2nd inert cycles performed at 900°C for oxygen carriers of $CaMn_aX_{1-a}O_{3-\delta}$ sintered at 1300°C.

3.2.1.1.2 The effect of operation temperature and production parameters

The ability of the oxygen carrier particles to release oxygen in the gas phase was also investigated at different temperatures using the C50MT7Mg3, C51MMg3 and C52MMg6 materials. The oxygen carrier particles were exposed to 100% N_2 flow for 360 s as presented in the section above. For each inert cycle, the oxygen concentration at the end of 360 s was

collected to gauge the CLOU property. An average value over two cycles was used and shown as a function of temperature in Figure 8 for the investigated material. Detailed experimental procedure can be found in Paper III.

As can be seen in Figure 8, operational temperature didn't influence the materials' CLOU properties in a significant way. The uncoupling behavior was relatively stable independent of temperature, although there is a clear drop at the highest temperature of 1050°C for C51MMg3 and C52MMg6. For these two materials. the lower concentration of released oxygen for 950°C (2) cycles, i.e. the cycles performed at 950°C after 1050°C cycles, are somewhat lower than the one at 950°C (1), which was conducted prior to the 1050°C cycles. This may indicate some deactivation of the material at the higher temperature due to the formation of $CaMn_2O_4$ which is a decomposition product of $CaMnO_{3-\delta}$ [105]. The C51MMg3 samples containing less MgO released a little bit more oxygen at temperatures lower than 1050°C. For C50MT7Mg3 material, the deactivation after higher temperature cycles did not seem to occur. The concentration of released oxygen was almost identical for 950°C (2) and 950°C (1) cycles. The O_2 concentration at 950°C (2) cycles achieved at C50MT7Mg3 was obviously higher compared with the other two materials. This suggests that the incorporation of Ti could improve the stability of the $CaMnO_{3-\delta}$ oxygen carrier.

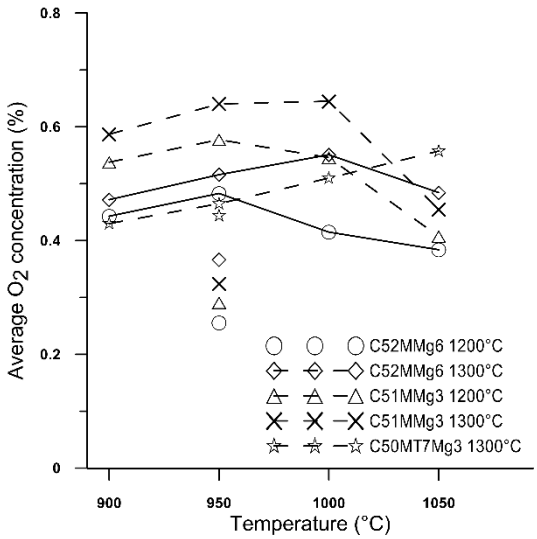

Figure 8. Released gaseous oxygen concentrations at the end of 360 s inert period of C50MT7Mg3, C51MMg3 and C52MMg6 oxygen carriers at different temperatures. The symbols separated from the lines present the results for the second 950°C period, which is performed after tests at 1050°C.

In the spray drying process of oxygen carrier particles, the milling time of for the prepared slurry, calcination temperature and time for the spray dried particles are important production parameters which could affect the property of produced oxygen carriers. The influence of these

three production parameters was studied in this thesis, see attached Paper IV for details, on the C51MMg3 oxygen carrier. Here, the CLOU property of examined oxygen carrier is presented.

In general, as seen in Figure 9, the concentration of released O_2 at 900°C was very similar for the investigated oxygen carriers. So the examined parameters, i.e. calcination temperature, time and milling time, does not have an obvious influence on the concentration of oxygen released. However, it can be noticed that the oxygen concentration obtained after fuel cycles was slightly lower than the concentration before the fuel cycles. It is important to consider that the oxygen release during the inert period is influenced by the state of the oxygen carrier during the oxidation, as the 3-δ is affected by the surrounding partial pressure of oxygen. Considering that the fresh particles were calcined and cooled to room temperature in air, there could be some particles still at a higher oxidation state, though they were exposed to 5% O_2 before exposing to 100% N_2.

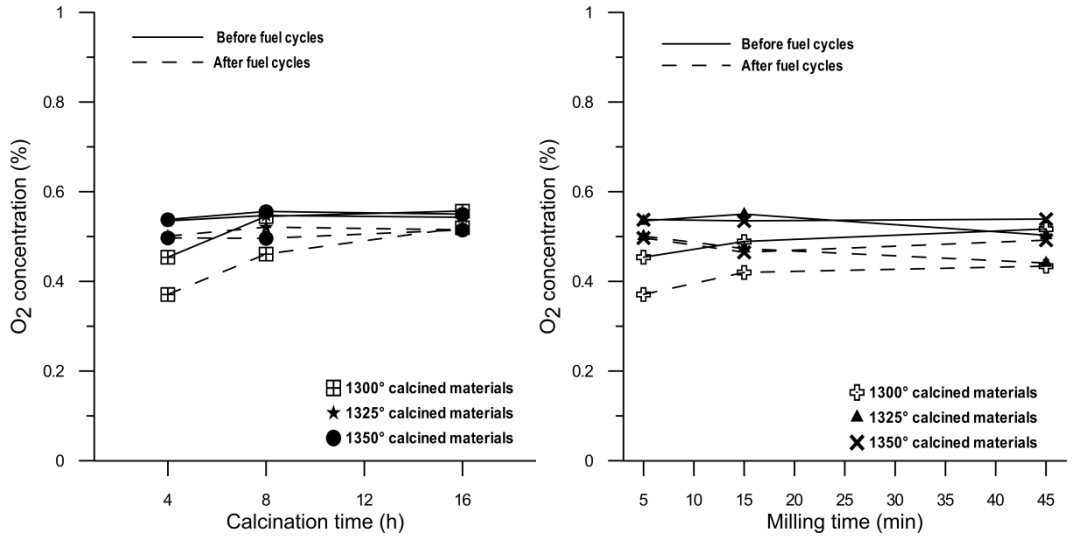

Figure 9. The average O_2 concentration at t=360 s of N_2 cycles at 900ºC for C51MMg3 oxygen carrier (a): milled for 5 min and (b): calcined for 4 h.

3.2.1.1.3 The effect of raw materials

To apply oxygen carrier material to a commercial scale chemical-looping unit, one key challenge is to find cheap raw materials available in large quantities for material production. As discussed in previous section and in section 3.3.1.2, C50MT7Mg3 material with molar composition $CaMn_{0.775}Mg_{0.1}Ti_{0.125}O_{3-\delta}$ did not suffer deactivation problem after high temperature cycles in batch reactor system tests. Moreover, in a 300 W_{th} continuous CLC unit, oxygen carrier C50MT7Mg3 showed better performance than C51MMg3 (molar composition $CaMn_{0.9}Mg_{0.1}O_{3-\delta}$) material which is likely a candidate material for large scale operation [101, 106]. Thus, the synthesis composition of C50MT7Mg3 material, i.e. 50.3 wt% $Ca(OH)_2$, 40.1

wt% Mn_3O_4, 6.8 wt% TiO_2 and 2.7 wt% MgO, was applied to investigate the effect of raw material on the important properties of the oxygen carrier. Considering the content and price, Mn- and Ti-oxides are likely the raw materials which will have the major effect on the cost. In Paper V, a large number of Mn-materials were obtained from various global suppliers, and twelve Mn-oxide sources were used in the production process. Further, four different TiO_2 powders were evaluated as well. Table 6 shows the raw powders which were used during the production. Mn-oxide source T and TiO_2 source A are chemical grade products, and they were used for the production of the calcium manganite oxygen carrier presented in previous sections, and are the reference materials. To study the effect of the raw materials, only one source, i.e. Mn-oxide or TiO_2 source, was altered at a time while keeping the other one as the reference. For instance, to examine the different Mn-oxide sources, the TiO_2 source used for oxygen carrier production was kept as A. Similarly, when study the different TiO_2 sources, the Mn-oxide sources used for oxygen carrier production was kept as T.

Table 6a. *Information of Mn-oxide sources*

Notation	Mn-oxide Source	Mn oxide	wt% Mn-oxide	Main impurity elements*
T	Trimanox (Reference)	Mn_3O_4	>99	/
A1	N60, Autlan	MnO_2	71	Fe, Si, Al, Ca
A2	N65, Autlan	MnO_2	71	Fe, Si, Al, Ca
B	BassTech	MnO	>98	/
C1	CDMA	MnO_2	81	Fe, Si, Al
C2	LM type	Mn_3O_4	94	Fe, Si, Al, P
C3	XH1452	MnO	N.A	N.A
E1	Colormax P	Mn_3O_4	96	Fe
E2	Colormax S	Mn_3O_4	96	Fe
E3	Micromax S, Elkem	Mn_3O_4	90-97	Fe
M	XH1455	MnO_2	N.A	N.A
N	(NDA)	MnO_2	N.A	N.A
S	Mangalox K45	MnO_2	79	Fe,Al

Note: *All impurities are in oxide phases.

Table 6b. *Information of TiO_2 sources*

Notation	TiO_2 Source	TiO_2 oxide	wt% TiO_2
A	Alfa Aesar (Reference)	Rutile TiO_2	99.9
C	AT-1, Cristal	Anatase TiO_2	98.7
K	Kronos 2900	Rutile TiO_2	>98.5
S1	Sachtleben TR	Rutile TiO_2	>99
S2	Sachtleben M211	Anatase TiO_2	>99

All examined oxygen carriers had the same molar composition $CaMn_{0.775}Mg_{0.1}Ti_{0.125}O_{3-\delta}$ and were calcined at 1350ºC for 4 h. The difference is the raw materials used, which is given in the notation of the oxygen carrier. For instance, oxygen carrier with notation A2A-1350 means that this oxygen carrier is produced from Mn oxide source A2 and TiO_2 source A and calcined at 1350ºC. The reference material, Ref.-1350, was produced from Mn oxide source T and TiO_2 oxide A, both of which are relatively chemically pure and expensive. Further, these materials are not likely available at sufficient scale to be of interest for an industrial application.

Perovskite structure $Ca(Mn_x,Ti_{1-x})O_{3-\delta}$ was identified by XRD in all fresh materials, see section 3.4 for details. So by using raw materials available in large quantity, the perovskite calcium manganite can be successfully produced. This shows that the material is rather simple to produce and there is a flexibility to what raw materials are used in the production process.

In Figure 10a and 10b, the oxygen concentration in the dry flue gas is plotted as a function of time for the 2nd inert cycle at 950°C for some of the oxygen carriers. In Figure 10c and 10d, the oxygen concentration profile at different temperatures was presented for the Ref.-1350 and E1A-1350 materials. In Figure 10, the dashed lines (blank) present the results of an experiment using a sand bed and the red solid lines (Ref.-1350) are the results from the reference material. All investigated oxygen carriers, including those not shown in the figure, had a similar oxygen concentration profile at examined experimental temperatures. So, under experimental conditions, the use of raw materials available in tonnage scale did not seem to influence the CLOU property of $CaMn_{0.775}Mg_{0.1}Ti_{0.125}O_{3-\delta}$ oxygen carrier. It should be considered that the profiles seen in Figure 10 may be limited by thermodynamics, since the profiles are the same for all studied samples. The rate of release in a fuel reactor may be significantly more rapid, and here there may be changes with respect to the uncoupling rate of the different materials. A solid fuel experiment was conducted on one material, showing a much faster rate of release of oxygen when exposed to fuel, in this case char. However, no comparison between different materials was made in this work.

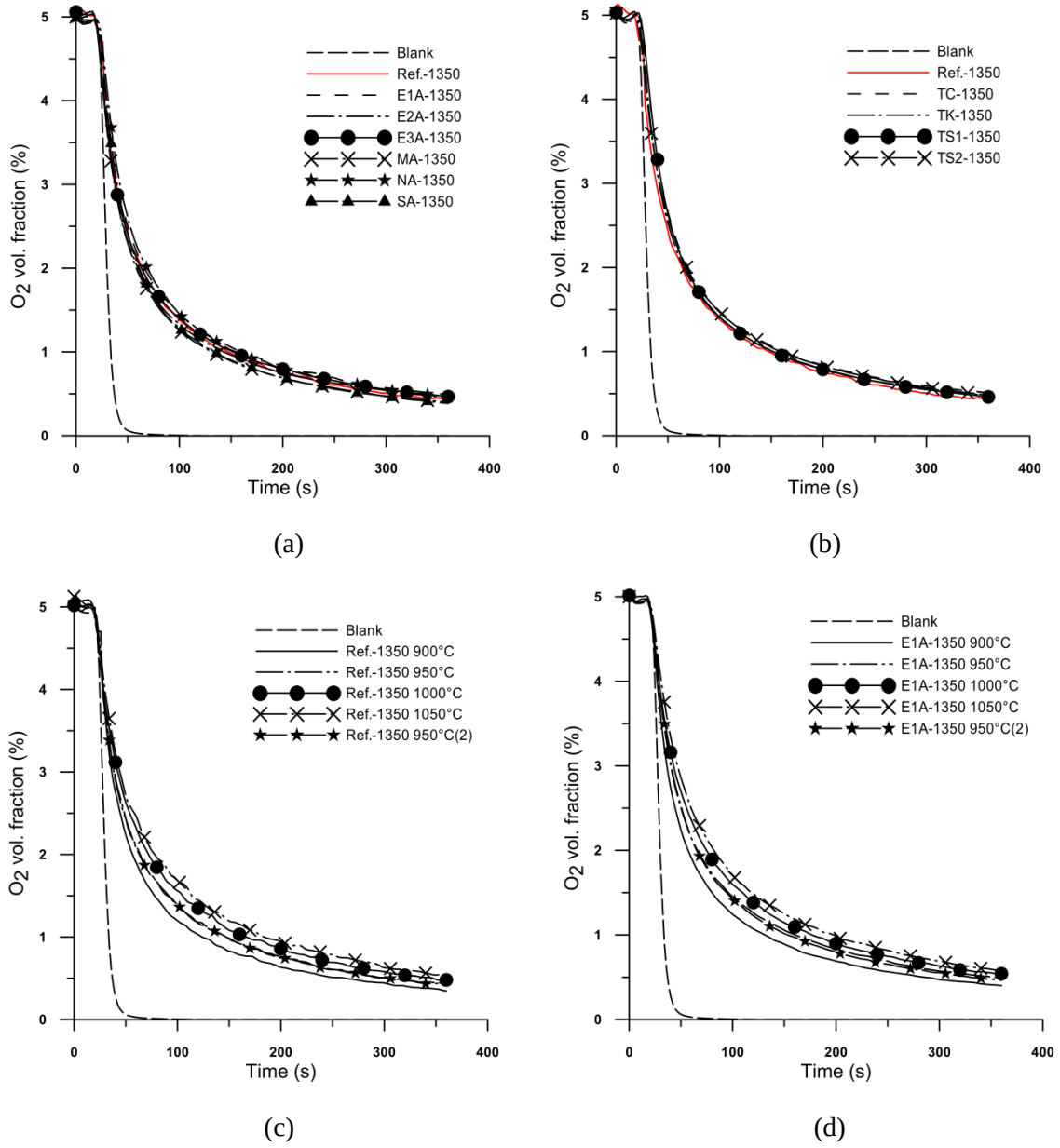

Figure 10. The O_2 volume fraction profile in inert cycles: (a) for oxygen carriers produced from different Mn-oxides sources, (b) for oxygen carriers produced from different TiO_2 sources. The experimental temperature was 950°C, (c) (d) shows similar profiles for Ref.-1350 and E1A-1350 at five reaction temperatures.

3.2.1.2 Mn-Si-O system

In this series of materials, SiO_2 was mixed with Mn_3O_4 to form combined Mn-Si oxides. The SiO_2 content in the particles was set to 2 wt%, 6 wt%, 10 wt%, 15 wt%, 20 wt%, 25 wt%, 30 wt%, 35 wt%, 45 wt%, 50 wt% and 75 wt%, which corresponds to a Si/(Mn+Si) molar ratio between 3% and 79%, see Table 3. The calcination temperature for the materials was 1050°C and 1150°C, and particles were calcined for 4 h at corresponding temperature. Batch reactor system tests were conducted at temperature 900-1100°C, see attached Paper VI.

Figure 11 shows the oxygen concentration after 360 s of inert period as a function of the Si/(Mn+Si) molar ratio at different temperatures. Clearly, the release characteristics are a function of calcination temperature, reaction temperature and composition.

For materials with a Si/(Si+Mn) ratio of less or equal to 0.40 there was a rather substantial release increase as the temperature was increased, with the best CLOU behaviour seen for the particles sintered at 1150°C. However, for oxygen carriers containing higher fractions of Si, there is practically no release of O_2 independent of reaction temperature for the particles sintered at the higher temperature, i.e. 1150°C.

According to the XRD results, see section 3.4, braunite Mn_7SiO_{12} together with bixbyite Mn_2O_3 or hausmannite Mn_3O_4 were the main phases in the 1050°C calcined fresh materials. But for material calcined at 1150°C, braunite Mn_7SiO_{12} was identified as the main phase. According to reaction 7, braunite is the main phase contributing to CLOU behaviour. The lack of braunite in the composition may be the reason for the limited CLOU property for the 1050 °C sintered Mn-Si materials.

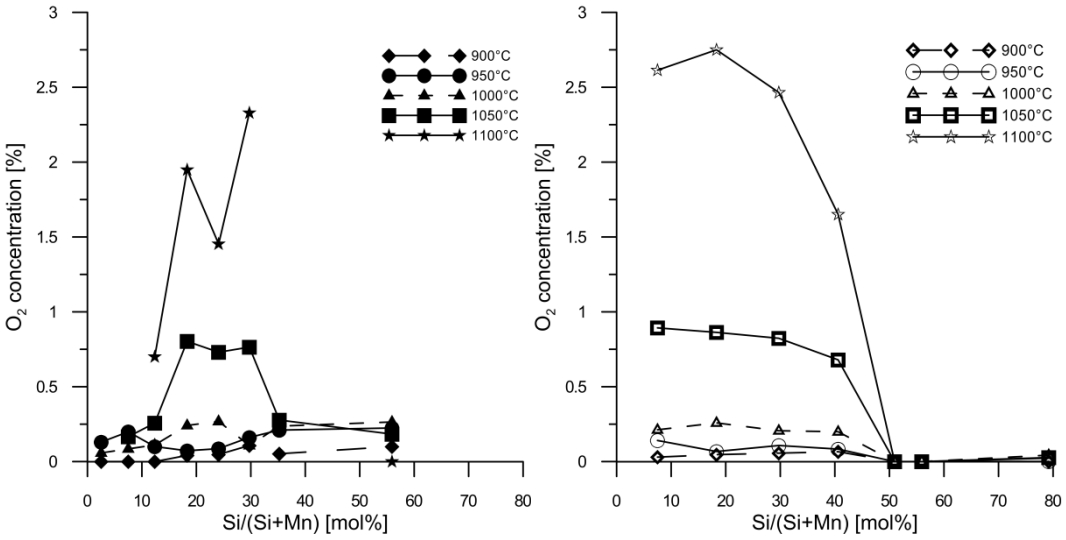

Figure 11. Oxygen concentrations after 360 s inert gas cycles at different temperatures as a function of the Si content for oxygen carriers calcined at (left) 1050°C and (right) 1150°C.

3.2.1.3 Mn-Mg-O system

Magnesium is another element that can be mixed with manganese in order to create particles with CLOU properties. This was proposed by Shulman et al., but only one composition was studied, using a Mn/Mg=1 [78]. Three compositions were designed with 21 wt%, 26 wt% and 35 wt% of MgO where the molar ratio of Mn/Mg is 2, 1.5 and 1 respectively. Each batch of oxygen carrier was sintered at 1200°C and 1300°C after spray-drying.

As shown in Figure 12, MMg35, which had the highest MgO content, released most oxygen to the gas phase. The oxygen concentration at the end of 360 s for 1200°C and 1300°C sintered sample was 0.6% and 0.3%. It should be mentioned that the levels of oxygen released at the conditions used in this work are relatively low, i.e. less than 3% at the conditions employed in these experiments. However, as was mentioned above, when fuel is introduced to the bed of oxygen carriers and remove the gas phase oxygen, the driving force for further release will increase, hence promoting the overall fuel conversion process. This is especially true in the case where the outlet concentration approaches equilibrium during the inert period, for instance with CuO.

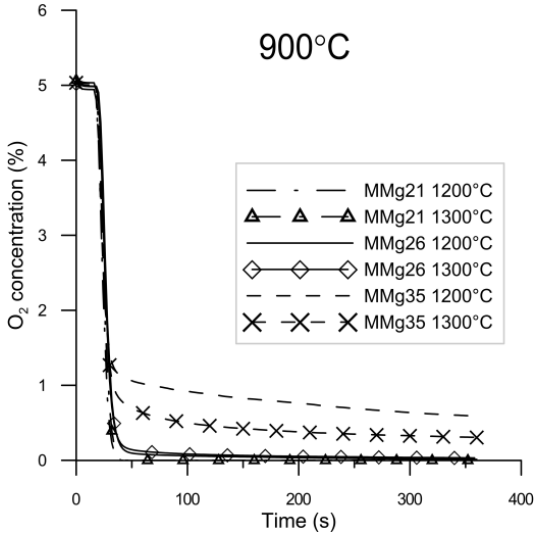

Figure 12. The O_2 concentration profile of the 2nd inert cycle performed at 900°C on Mn-Mg-O materials.

3.2.2 CuO based system

CuO is known for its high oxygen transfer capacity and fast oxygen uncoupling reaction rate when used as oxygen carrier [21, 70, 107]. In this work, 12 kinds of CuO-based oxygen carriers were manufactured and examined. The CuO weight percentage varied from 36% to 60% and the selected support materials were ZrO_2-, CeO_2-, $MgAl_2O_4$-and Fe-based materials.

In the experiment to evaluate the uncoupling behaviour, the CuO-based particles were exposed to 100% N_2 environment for 360 s after being fully oxidized. Figure 13 shows the outlet O_2 concentration as a function of time for experiments conducted at 900°C. At t=0 s, the oxygen was shut off and 100% N_2 was injected into the system. The oxygen concentration stayed at 5% for about 20 s, and is due to the delay-time in the reactor system. Then the oxygen concentration dropped sharply since the oxygen was flushed out by the injected N_2. At about t=30 s, the oxygen concentration in the outlet was stable at around 1% for most of the CuO-based materials. The released oxygen resulted from the CLOU property of the CuO and the oxygen was released according to reaction 5. At 900°C, the calculated equilibrium oxygen concentration for CuO to

Cu_2O is 1.4%, see Table 5, which is slightly higher than 1% observed for most of the tested CuO. Lower temperature in the bed than the set value for oven control could be a reason for the discrepancy, as the very constant release rates suggest equilibrium control.

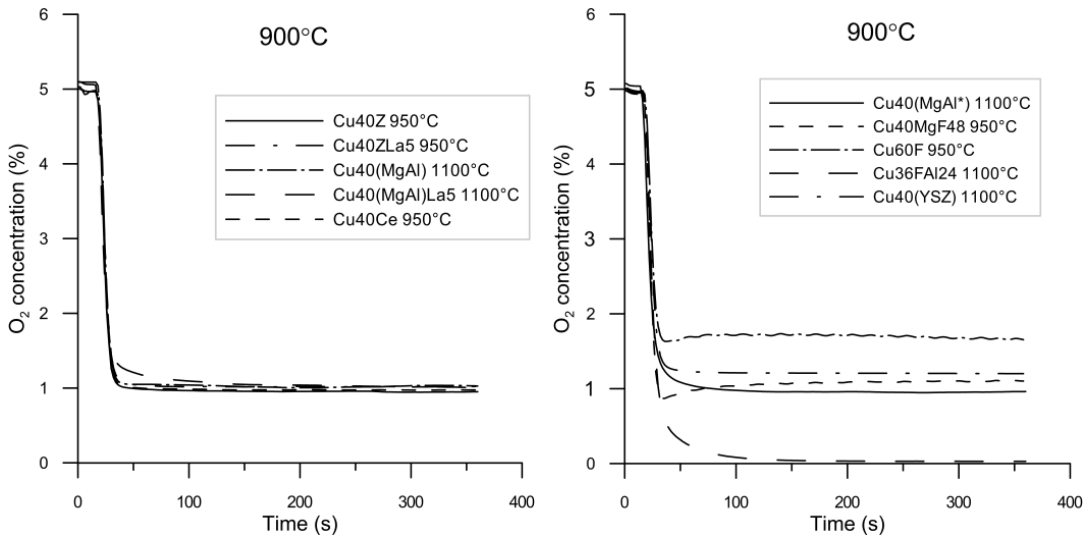

Figure 13. The O_2 concentration profile of the 2nd inert cycles performed at 900°C for CuO-based materials.

As seen in Figure 13, Most of the CuO-based materials showed similar CLOU property at 900°C and released about 1% O_2 to the gas phase during 360 s of N_2 flushing. The Cu60F 950°C sample released more oxygen compared to the other tested materials. Instead of reducing CuO to Cu_2O, a possible CLOU mechanism for Cu60F material could be the reaction between CuO and $CuFe_2O_4$ which forms delafossite $CuFeO_2$, see reaction 16. Jacob et al. proposed that the oxygen partial pressure for reaction 16 is higher than reaction 5 [108], which could explain this result.

$$CuO + CuFe_2O_4 \rightarrow 2CuFeO_2 + ½\ O_2(g) \qquad (16)$$

Sample Cu36FAl24 released almost no oxygen under tested condition. It was identified that there was no CuO phase in the sample as all the CuO reacted with Fe_2O_3 and Al_2O_3 forming $Cu_{0.95}Fe_{1.05}AlO_4$, see section 3.4. Considering that there was no available CuO phase, the low CLOU propensity of this material was not altogether surprising.

3.3 Reactivity with fuels (methane and syngas)

Most oxygen carriers were evaluated using methane and syngas. Methane, the main compound in natural gas, is a common gaseous fuel used for generation of electricity in power plants. Syngas, which contains both CO and H_2, is a product from gasification and can be used as

gaseous fuel for CLC. It is also an important intermediate when employing solid fuels in CLC. These two fuels were chosen to study the reactivity of oxygen carriers.

At 950ºC in the batch fluidized bed test, full syngas conversion (100% conversion of CO to CO_2 and H_2 to H_2O) was achieved on all examined oxygen carriers, except MSi45-1150, MSi50-1150 and MSi75-1150 samples. Thus, the discussion of oxygen carrier's reactivity focuses on its conversion of CH_4.

3.3.1 Combined manganese oxides

3.3.1.1 Perovskite Ca-Mn-X-O (X=Fe, Ti and Mg) system

3.3.1.1.1 The effect of additives

In general, the perovskite materials were very reactive towards CH_4. Figure 14 demonstrates the CH_4 conversion as a function of oxygen carrier conversion for these materials. At 950°C, the perovskite type materials achieved over 85% methane conversion using an oxygen carrier mass to fuel flow corresponding to 57 kg/MW. Full conversion was obtained on sample C49MF5, C51MMg3 and C52MMg6. From the screening study of these calcium manganites, see Paper II, the $CaMn_{1-x}Mg_xO_{3-\delta}$ was deemed most promising and investigated more extensively in Paper III and IV. It is worth to mention that the other non-perovskite Ca-Mn-X-O (X=Fe, Ti and Mg) oxygen carriers showed lower methane reactivity, see Paper I.

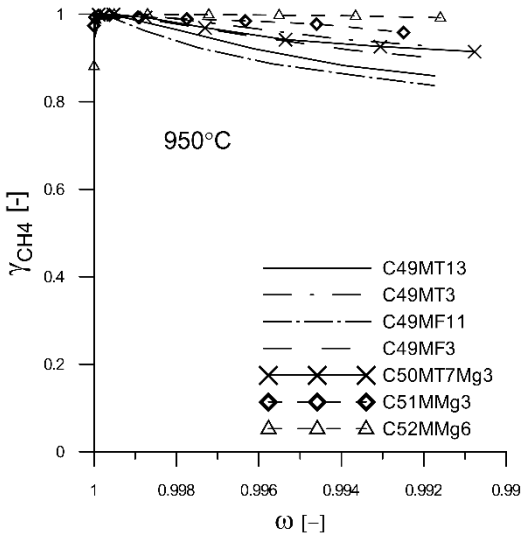

Figure 14. Methane conversion as a function of solid conversion of the 2nd methane cycle at 950°C for 1300°C sintered perovskite Ca-Mn-X-O materials.

3.3.1.1.2 The effect of operation temperature and production parameters

The effect of operation temperature on the reactivity of oxygen carriers was carried on the C50MT7Mg3 (molar composition $CaMn_{0.775}Mg_{0.1}Ti_{0.125}O_{3-\delta}$), C51MMg3 (molar composition:

$CaMn_{0.9}Mg_{0.1}O_{3-\delta}$) and C52MMg6 (molar composition $CaMn_{0.8}Mg_{0.2}O_{3-\delta}$) oxygen carriers. Most of the results can be found in Paper III. The temperature influence is clearly seen in Figure 15. When the temperature was increased from 900°C to 950°C, a clear improvement in the methane conversion was achieved. At 950°C, methane conversion of oxygen carriers examined are very high: about 99% for C51MMg3 and C52MMg6 and about 93% for C50MT7Mg3 material. The positive effect of temperature on methane conversion is clearly seen on C50MT7Mg3 sample. While for the C51MMg3 and C52MMg6 materials, methane conversion at 950ºC is already around 99%, making it hard to see the effect of further temperature change. The methane yield at 1000°C is a little bit lower than 950°C for the oxygen carrier C52MMg6 1300, but the difference is very small. Although high temperature improves methane conversion, it may cause deactivation of the oxygen-carrier reactivity. This was examined by comparing the reactivity at 950°C, before (1) and after (2) testing at the maximum temperature of 1050ºC. For C51MMg3 and C52MMg6 materials, the particles reactivity at 950°C (1) (symbol on the line) is apparently higher than the one for 950°C (2) (the single symbol separated from the line). This indicates that materials suffer some deactivation, likely caused during the high temperature cycles. But for C50MT7Mg3 material, instead of deactivation, an increase of reactivity was observed at 950°C (2) as seen in Figure 10. So incorporation of Ti into the perovskite structured $CaMnO_{3-\delta}$ has a positive effect on material's reactivity as well.

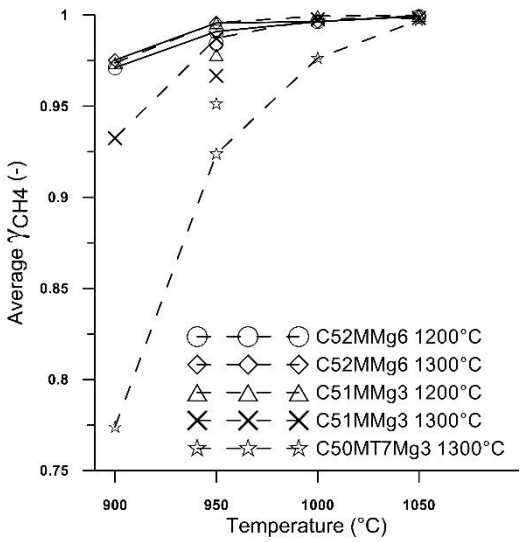

Figure 15. The average methane yield of C50MT7Mg3, C51MMg3 and C52MMg6 oxygen carriers as a function of temperature (data was selected for ω from 1 to 0.99). The single symbols are the results for the cycles at 950°C following high temperatures cycles.

The influence of production parameters, i.e. calcination temperature, calcination time and milling time, was studied on the C51MMg3 oxygen carrier in Paper IV. The CH_4 conversion at 950°C of investigated oxygen carriers is summarized in Figure 16. For particles with milling time of 5 min, the effect of calcination temperature and calcination time on the reactivity of

materials can be studied in Figure 16a. The CH_4 conversion as a function of milling time is presented in in Figure 16b for materials calcined for 4 h.

For the oxygen carriers calcined for 4 h and 8 h it is clear that increasing the calcination temperature from 1300°C caused a decrease of the material's reactivity towards CH_4, see Figure 16a. Comparing the reactivity of 1300C4h5m and 1325C4h5m, an increase of calcination temperature by 25°C resulted in as much as 40% lower CH_4 conversion. The two oxygen carriers calcined at the two highest temperatures had similar reactivity, which varied somewhat depending upon calcination time. The material calcined at 1350°C actually had somewhat higher conversion compared to material sintered at 1325°C. Interestingly the reactivity for all materials converge at around 60% conversion at the longest calcination time.

Prolonged ball-milling time had a negative effect on the particle reactivity. The only exception was for the material sintered at 1325ºC when the milling time was increased from 5 min to 15 min. Oxygen carriers with 15 min and 45 min milling time both achieved higher CH_4 conversion at 950°C. As was noted previously in Figure 5, a change in the production procedure also changes the physical characteristics of the oxygen carrier particles. There is a general relationship of decreasing reactivity with increasing crushing strength, although not all particles show this behaviour. Further, it is possible to find an optimum type of particle with a combination of reasonable crushing strength and high reactivity. For instance, the sample calcined at 1300ºC for 8 h with milling time 5 min had a crushing strength of 4 N and a gas yield of 86%.

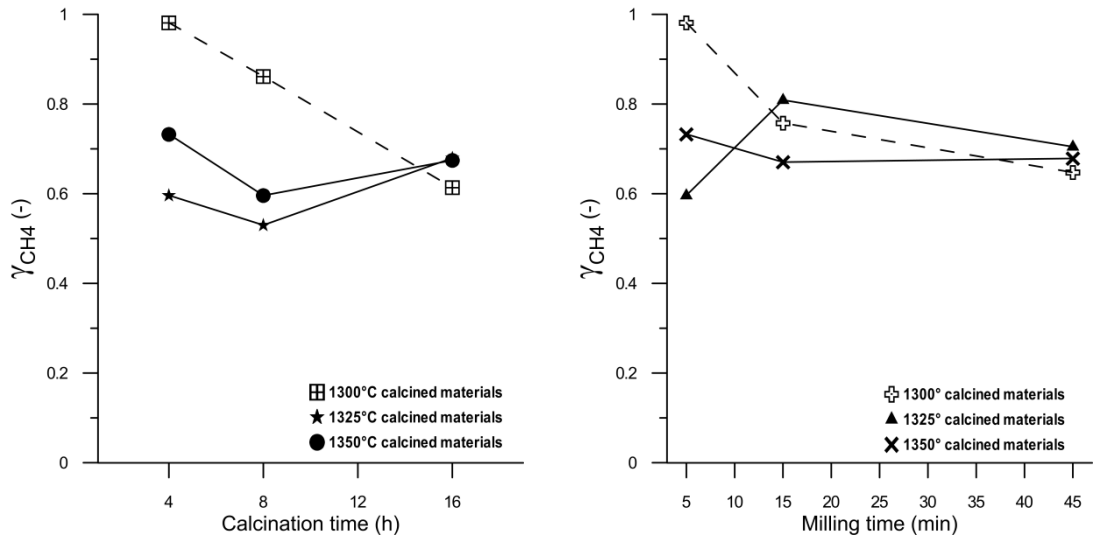

(a) (b)

Figure 16. The CH_4 conversion at 950°C for: (a) oxygen carriers with 5 min milling time; (b) oxygen carriers calcined for 4 h.

3.3.1.1.3 The effect of raw materials

In Paper V, twelve Mn-oxide sources and four TiO_2 sources were selected for the production of C50MT7Mg3 (raw material composition: 50.3 wt% $Ca(OH)_2$, 40.1 wt% Mn_3O_4, 2.7 wt% MgO and 6.8 wt% TiO_2). The strategy used for screening the effect of different source materials is discussed in section 3.2.1.1.3. To make a comparison between oxygen carriers, the methane conversion was calculated as an average in a ω range 1~0.99. In Figure 17, the average methane conversion as a function of experimental temperature is given. Although all materials had the same crystalline phases, see section 3.4, there is a difference in methane conversion with respect to the raw Mn-oxide source used. The samples that had comparable or better reactivity than the reference material were BA-1350, C2A-1350, C3A-1350, E1A-1350, NA-1350 and SA-1350.

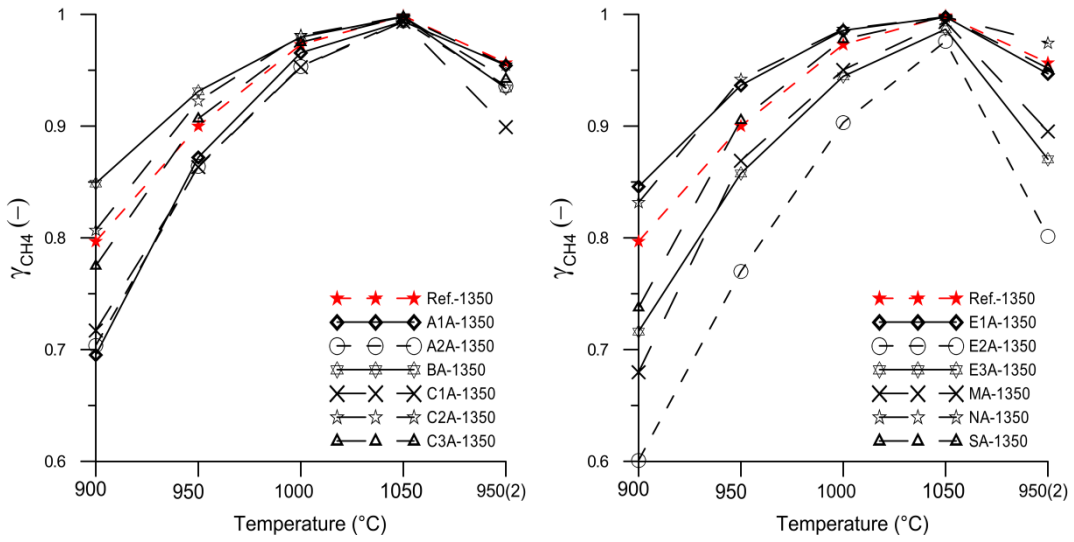

(a) (b)

Figure 17. Average methane conversion as a function of temperature for oxygen carriers of $CaMn_{0.775}Mg_{0.1}Ti_{0.125}O_{3-\delta}$ produced from different Mn-oxides.

The methane conversion of the oxygen carriers was also influenced by the TiO_2 source used. When TiO_2 source C, K and S1, see in Table 1 and 2 in Paper V, replaced the reference TiO_2, the methane conversion decreased significantly, with a minimum of around 45% at 900°C, which is observed in Figure 18. However, the material TS2-1350 produced from TiO_2 source S2 had somewhat better methane conversion compared with the reference material.

From the initial screening study of utilization of different Mn- and Ti-sources, one material was produced using a combination of the most promising Mn_3O_4 source E1 and TiO_2 source S2. This material was calcined at different temperatures in the temperature range 1325-1350°C, and it was found that the best particles were obtained at 1335°C, where a combination of high methane reactivity and crushing strength was obtained. These results are described in more detail in Paper V.

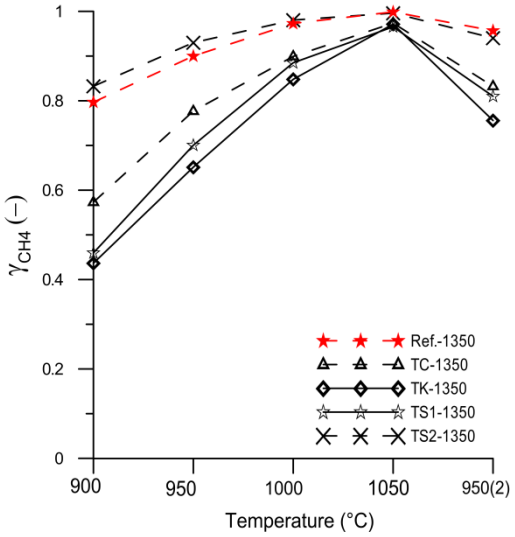

Figure 18. The average methane conversion as a function of temperature for of $CaMn_{0.775}Mg_{0.1}Ti_{0.125}O_{3-\delta}$ oxygen carriers produced from different TiO_2 sources.

3.3.1.2 Mn-Si-O system

Figure 19 summarized the average CH_4 conversion as a function of Si/(Mn+Si) molar ratio at five examined temperatures. For the samples with a Si/(Mn+Si) molar ratio less than 40%, the CH_4 conversion increases with temperature in the range 900°C to 1050°C for both 1050°C sintered (left in Figure 19) and 1150°C sintered (right in Figure 19) samples. At 1100°C, deactivation or defluidization occurred on some of the materials calcined at the lower temperature and containing low concentrations of Si. On the other hand, 1150°C sintered samples with Si/(Mn+Si) molar ratio less than 40% maintained high performance at 1100°C. There is a clear deactivation in reactivity for samples containing more than 50 mol% Si, and is in conformity with the low CLOU activity seen for these materials. The reactivity of 1150°C sintered MSi45, MSi50 and MSi75 was very low, less than 10% CH_4 conversion, at all examined temperatures. Although the MSi50 sample sintered at 1050°C had better reactivity compared to its 1150°C counterpart, also here there are clear tendencies towards reactivity loss at high temperatures.

The deactivation and defluidization problem detected on 1050°C sintered particles at higher temperatures may be due to a post-sintering effect during experiments. At 1050°C and 1100°C, where the experimental temperature was the same or higher than the sintering temperature for these materials, the particles might start to melt, forming agglomerates or other unreactive phases at the high reaction temperature. Soft agglomerations which could easily be broken apart could be an evidence for the post-sintering effect.

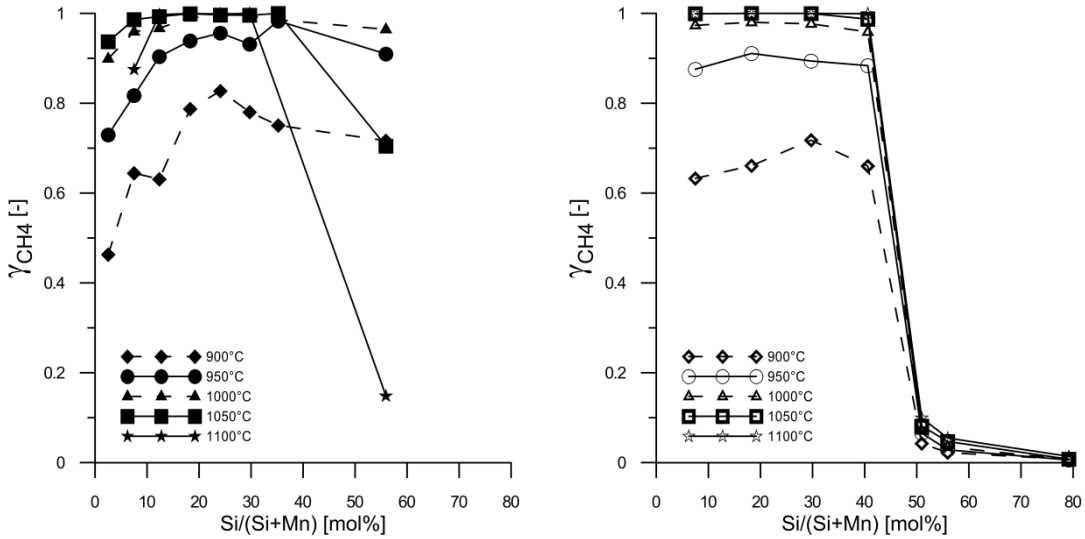

Figure 19. Methane conversion as a function of solid conversion at different temperatures as a function of the Si content for oxygen carriers calcined at (left) 1050ºC and (right) 1150ºC.

3.3.1.3 Mn-Mg-O system

The reactivity of the Mn-Mg-O particles as a function of solid conversion is presented in Figure 20. It is clearly demonstrated that the reactivity towards methane increased with increasing Mg content. MMg35, with an equal molar amount of Mn and Mg, released most gaseous oxygen had the highest methane conversion at 950°C followed by MMg26 and MMg21. It can also easily read from Figure 20 that the particles sintered at 1300°C showed lower reactivity compared with the particles having the same composition but sintered at 1200°C. The reason could be that the particles sintered at higher temperatures are denser and the surface area is probably smaller. A lower porosity may lead to lower gas-solid reaction rates, but a detailed mechanism of this effect needs to be further studied.

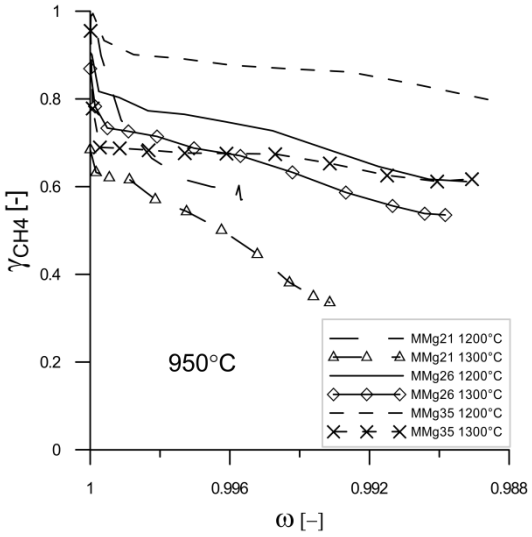

Figure 20. Methane conversion as a function of solid conversion of the 2nd methane cycles at 950°C for Mg-Mn-O materials.

3.3.2 CuO based system

CuO-based materials exhibited extraordinary reactivity towards CH_4 at the experimental conditions used here, i.e. 57 kg OC/MW and temperatures of 900°C and 925°C. Full methane conversion was achieved on 7 out of 10 CuO-based materials at 925°C, see Figure 21. The methane conversion of the remaining materials Cu60F, Cu40MgF48 and the Cu36FAl24 sample was 90%, 86% and 83% respectively, values which can be judged to be quite good at these experimental conditions compared to other non-CLOU type of oxygen carriers.

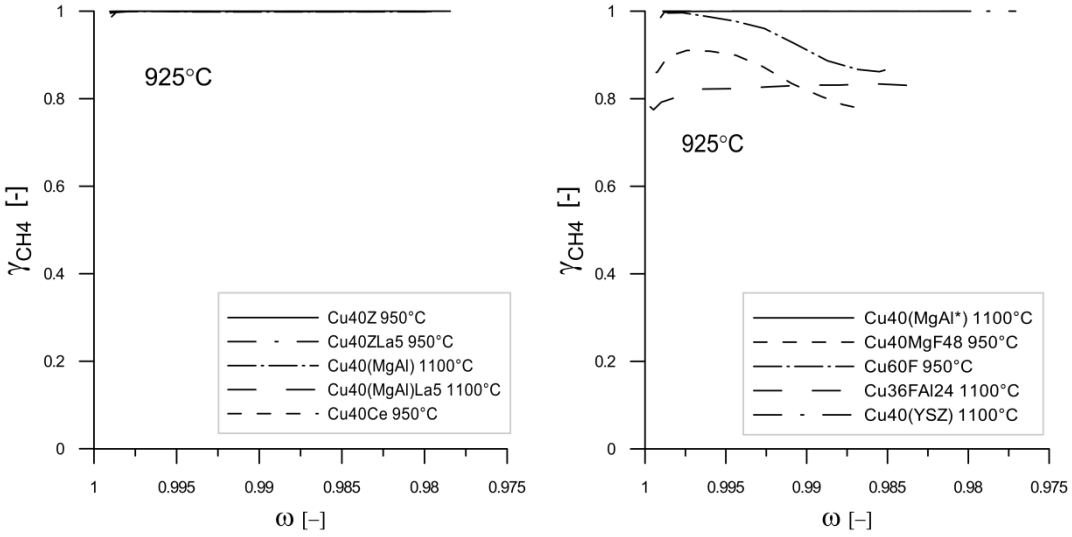

Figure 21. Methane conversion as a function of solid conversion for the 2nd methane cycle at 925°C performed on CuO-based materials. See Table 5 for exact composition.

3.4 Characterization

Oxygen-carrier materials studied in this work were generally highly spherical particles, which is expected from a spray-drying process. However some particles, for instance Cu40Ce 950°C, had holes at the center of the spheres forming so-called doughnut shape particles. This defect was caused by imperfect spray-drying, and should be possible to eliminate in an optimized process. Figure 22 presents the light microscopy image of C52MMg6 1300°C, MSi30 1050°C, MMg35 1200°C and Cu40Ce 950°C samples for demonstration of the general appearance of the type of particles studied in this work.

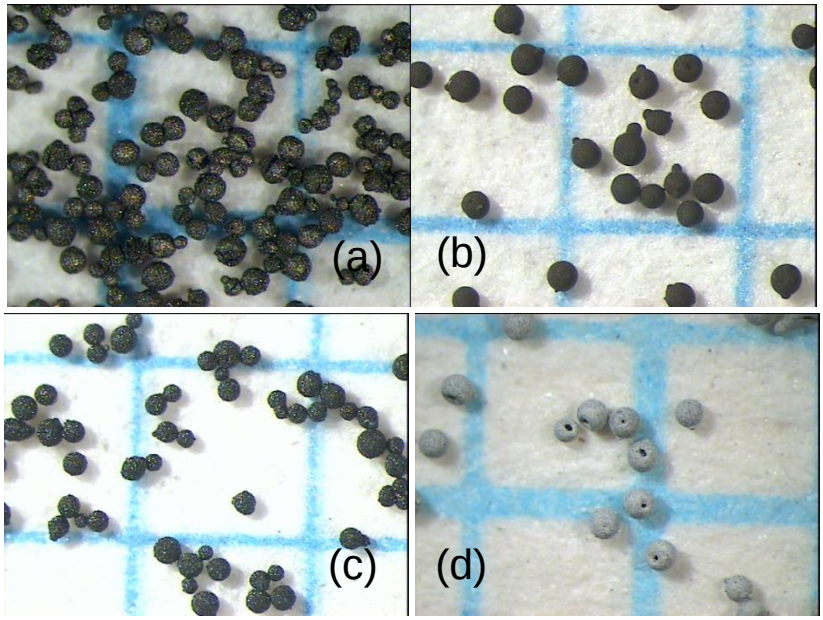

Figure 22. Light microscope pictures of fresh oxygen carriers with diameter 125-180 µm. The blue grids are 1 mm squares of the background millimetre paper. (a): C52MMg6 1300°C; (b): MSi30 1050°C; (c): MMg35 1200°C; (d): Cu40Ce 950°C.

The crystalline phases of examined oxygen carriers were identified by XRD. Normally both fresh and used particles were analysed. At the end of batch reactor system testing, particles were cooled down in 5% O_2 (compensated by N_2) from the reaction temperature to room temperature. These particles are referred as used samples. The identified phases in both fresh and used samples are summarized in the following tables.

The crystalline structure of Ca-Mn-X-O (X=Fe,Ti and Mg) oxygen carriers is summarized in Table 7. The perovskite type $CaMnO_{3-\delta}$ is the major phase identified in all samples. Although not presented in the fresh sample, $CaMn_2O_4$ was recognized in the used sample for some of the $CaMnO_{3-\delta}$ samples. For these perovskite $CaMnO_{3-\delta}$ oxygen carriers, creation of oxygen deficiency in the structure (increased δ value) is the mechanism of oxygen transportation [94, 95]. But the growth of deficiency can only occur within a certain range of oxidation states. When the degree of reduction is over a certain limit, $CaMnO_{3-\delta}$ decomposes and $CaMn_2O_4$ is a

possible decomposition product [94]. The formation of $CaMn_2O_4$ did cause some deactivation of the reactivity of some of these oxygen carriers, see Paper III for details. For the C51MMg3 and C52MMg6 samples, MgO existing in a separate phase, marked by red rings in Figure 23, was also confirmed by SEM/EDX.

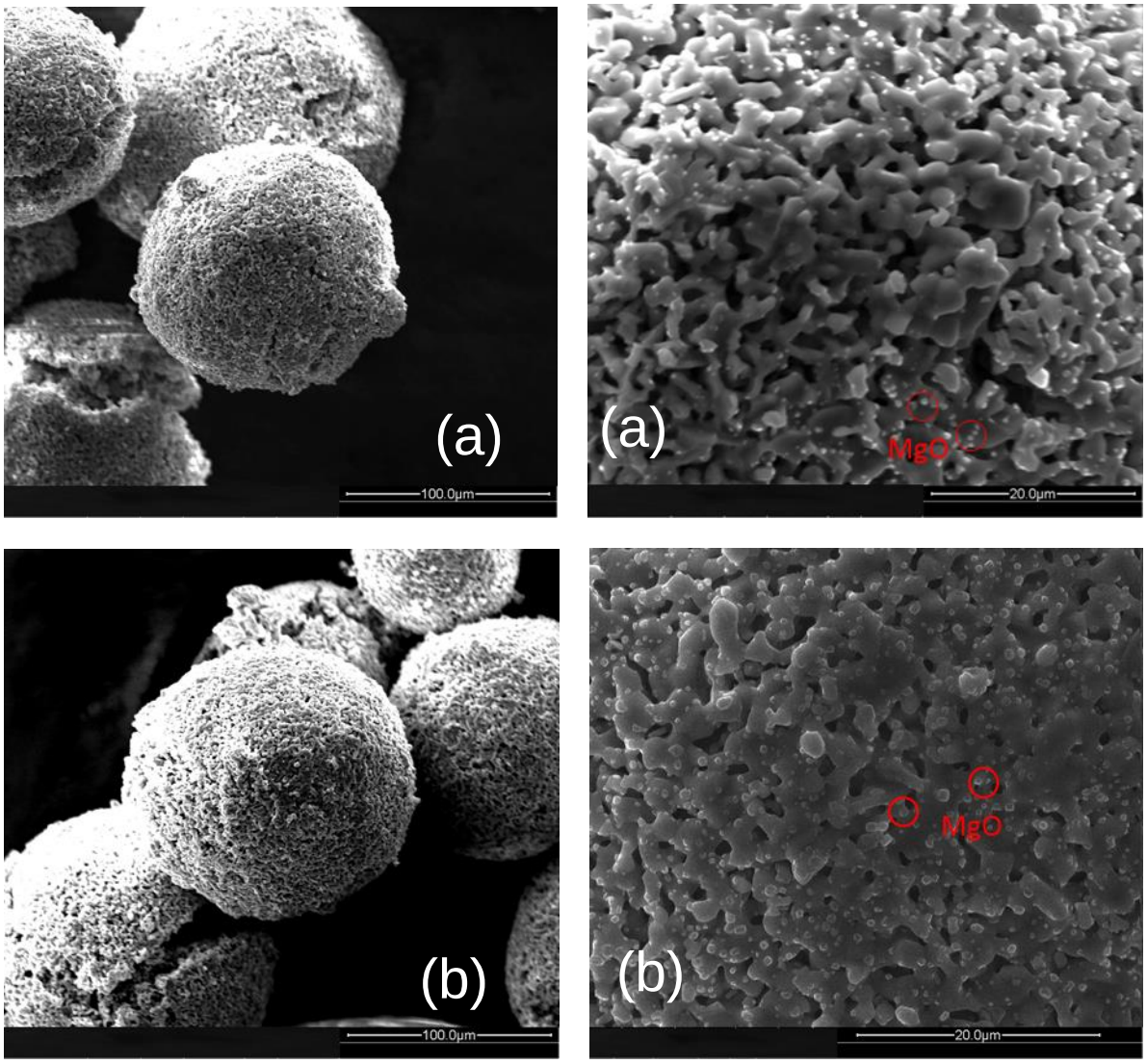

Figure 23. SEM image of C52MMg6 1300 sample. (a): fresh sample. (b): used sample (cooled down to room temperature by 5% O_2 in N_2)

The XRD diffraction pattern of C51MMg3 samples produced with different production parameters is shown in Figure 24. Three samples (both fresh and used ones) were chosen for demonstration here, but all samples had the same diffraction pattern. This means that the variation of investigated production parameters did not influence the perovskite crystalline structure of the calcium manganite oxygen carrier. For the C50MT7Mg3 oxygen carrier, the perovskite phase $CaMn_{0.9}Ti_{0.1}O_{3-\delta}$ was success fully produced in all samples regardless of the Mn-oxide/TiO_2 source used, see Paper V. So it is feasible to produce the perovskite calcium

manganite oxygen carrier by using of raw materials available in tonnage scale and with widely varying characteristics.

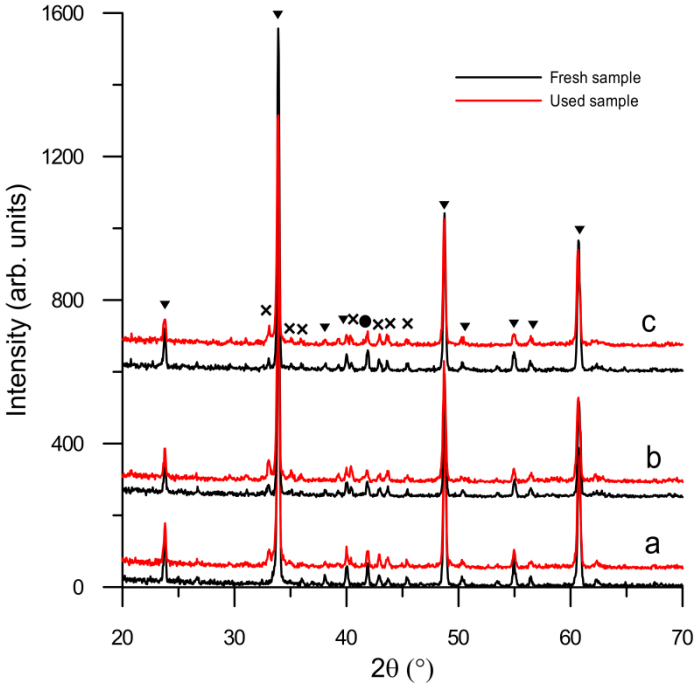

Figure 24. The XRD diffraction patterns of the C51MMg3 ($CaMn_{0.9}Mg_{0.1}O_{3-\delta}$) oxygen carrier with different production parameters: (a) 1300C4h5m, (b) 1300C4h15m and (c) 1300C4h45m sample. Fresh samples are presented by black lines and used samples were presented by red lines. Peaks of crystalline phase $CaMnO_{2.97}$ (▼), $CaMn_2O_4$ (✕) and MgO (●) are marked in the image.

Crystalline phases of the Mn-Si-O materials are summarized in Table 8. For particles calcined at 1050°C, manganese oxide in the form of bixbyite Mn_2O_3 was present in all samples except in MSi50-1050. After the reactivity test, hausmannite Mn_3O_4 appeared in the used samples instead of bixbyite Mn_2O_3. Fresh particles were calcined and cooled down to room temperature in air, while used samples were cooled down to room temperature under O_2 partial pressure of 0.05 atm. In air, Mn_2O_3 is thermodynamically more favoured than Mn_3O_4 at temperature below 800ºC. However, at an O_2 partial pressure of 0.05 atm, oxidation of Mn_3O_4 to Mn_2O_3 is hard to achieve, as described in section 1.2.1. This could explain why hausmannite Mn_3O_4 is found in the used sample, and not bixbyite. For fresh particles calcined at 1150°C, braunite Mn_7SiO_{12} or rhodonite $MnSiO_3$ were the main manganese-containing phases depending on the content of SiO_2. This suggests that higher sintering temperature facilitates the formation of manganese silicates. It is thus likely that the oxygen release mechanism is through reaction (5) as also suggested by the phase diagram.

In Table 9, it can be seen that Mg_2MnO_4 and $MgMn_2O_4$ were the phases present in the fresh MMg21 and MMg26 samples. After the experiments, only $MgMn_2O_4$ could be identified. For the MMg35 sample, Mg_2MnO_4 was the only phase in both fresh and used samples. According to reaction 8 and reaction 9, Mg_2MnO_4 can decompose to $MgMn_2O_4$, and $MgMn_2O_4$ can further

decompose to Mn_3O_4. Both of the reactions should release gaseous oxygen. But in our experiments, only MMg35 was observed to have significant CLOU behaviour and its reactivity was the highest among this series of materials. This may indicate that Mg_2MnO_4 is the active phase contributing to the oxygen uncoupling reaction rather than $MgMn_2O_4$. And under our experimental conditions, Mg_2MnO_4 is more reactive towards CH_4 than $MgMn_2O_4$. It is likely that the dominating oxygen release reaction is through Mg_2MnO_4 via reaction 8, which also implies a sliding equilibrium. So, for combined Mg-Mn oxygen carriers, it would seem as if oxygen carriers with higher content of Mg are most viable for a CLOU process.

Detected phases in the CuO-based materials are listed in Table 10. Phases in the fresh samples indicate the actual compounds in the oxygen carrier after synthesis. For 9 out of 10 samples, the active material was CuO in addition to the support. The exception to this was Cu36FAl24, which contained a single phase $Cu_{0.95}Fe_{1.05}AlO_4$. CuO on $MgFe_2O_4$ support had a similar oxygen equilibrium for CLOU reaction at 900°C, but were less reactive towards CH_4 compared to the other CuO-based materials except Cu36FAl24, see Figure 21. $MgFe_2O_4$ itself can be oxidized or reduced and was investigated as a catalyst for CH_4 combustion and other heterogeneous catalytic processes [109-111]. Hence, the reason for the lower reactivity of the $CuO/MgFe_2O_4$ oxygen carrier towards CH_4 needs to be further studied. For the Cu60F material, it has a different mechanism for oxygen release, as was described in section 3.2.2. This sample consists of CuO and $CuFe_2O_4$ which could form delafossite $CuFeO_2$, shown by reaction 16. As discussed before, reaction 16 has a higher oxygen partial pressure than reaction 5 [108]. This may explain the higher CLOU oxygen concentration at 900°C for the Cu60F sample. Since this material had higher oxygen partial pressure, one would expect that it has a higher reactivity as well. However, the sample's reactivity was relatively low in comparison to other Cu-based materials at these conditions, 90% methane conversion at 925ºC, which could be due to a lower rate of oxygen release from the particles, something which is not possible to discern from these experiments. For the Cu36FAl24 sample, no free CuO was found in the particles and its single phase compound $Cu_{0.95}Fe_{1.05}AlO_4$ did not have any observable CLOU property. However, $Cu_{0.95}Fe_{1.05}AlO_4$ was a reported oxygen carrier with over 90% CH_4 conversion at 900°C [57], and also in this work the oxygen carrier showed some reactivity towards methane, see Figure 21, although the reaction likely proceeds through normal CLC. A comparison of the phases in used sample and in fresh sample found that no extra phases were identified. This suggests that these materials had a good crystalline reversibility.

Table 7. *Identified crystalline phases of 1300°C sintered Ca-Mn-X-O(X=Cu, Fe, Ti and Mg) materials on which reactivity tests were successfully performed. The main phases were presented first followed by minor phases.*

Notation	**Raw materials** *(wt%)*	**Phases in fresh sample (calcined at 1300°C)**	**Phases in used sample**
C49MF5	49.2 $Ca(OH)_2$, 45.5 Mn_3O_4, 5.3 Fe_2O_3	$Ca(Mn,Fe)O_{3-\delta}$	$Ca(Mn,Fe)O_{3-\delta}$, $CaMn_2O_4$
C49MF11	49.0 $Ca(OH)_2$, 40.4 Mn_3O_4, 10.6 Fe_2O_3	$Ca(Mn,Fe)O_{3-\delta}$, $CaMn_2O_4$, Fe_2O_3	$Ca(Mn,Fe)O_{3-\delta}$, $CaMn_2O_4$
C49MT3	49.2 $Ca(OH)_2$, 48.1 Mn_3O_4, 2.6 TiO_2	$Ca(Mn,Ti)O_{3-\delta}$, $CaMn_2O_4$	$Ca(Mn,Fe)O_{3-\delta}$, $CaMn_2O_4$
C49MT13	49.0 $Ca(OH)_2$, 37.8 Mn_3O_4, 13.2 TiO_2	$Ca(Mn,Ti)O_{3-\delta}$, $CaMn_2O_4$	$Ca(Mn,Ti)O_{3-\delta}$, $CaMn_2O_4$
C51MMg3	50.5 $Ca(OH)_2$, 46.8 Mn_3O_4, 2.7 MgO	$CaMnO_{3-\delta}$, MgO	$CaMnO_{3-\delta}$, $CaMn_2O_4$, MgO
C52MMg6	51.8 $Ca(OH)_2$, 42.6 Mn_3O_4, 5.6 MgO	$CaMnO_{3-\delta}$, MgO	$CaMnO_{3-\delta}$, $CaMn_2O_4$, MgO

Table 8a. *Identified crystalline phases of parts of Mn-Si-O materials. Particles were sintered at 1050°C.The main phases were presented first followed by minor phases.*

Notation	**Raw materials (wt%)**	**Phases in fresh sample (calcined at 1050°C)**	**Phases in used sample**
MSi2	98 Mn_3O_4, 2 SiO_2	Mn_2O_3, Mn_3O_4	Mn_3O_4
MSi6	94 Mn_3O_4, 6 SiO_2	Mn_2O_3	Mn_3O_4
MSi10	90 Mn_3O_4, 10 SiO_2	Mn_7SiO_{12}, Mn_2O_3	Mn_3O_4
MSi15	85 Mn_3O_4, 15 SiO_2	Mn_7SiO_{12}, Mn_2O_3, SiO_2	Mn_7SiO_{12}, Mn_3O_4
MSi20	80 Mn_3O_4, 20 SiO_2	Mn_7SiO_{12}, Mn_2O_3,SiO_2	Mn_3O_4
MSi25	75 Mn_3O_4, 25 SiO_2	Mn_7SiO_{12}, Mn_2O_3, SiO_2	Mn_7SiO_{12}, Mn_3O_4, $MnSiO_3$
MSi30	70 Mn_3O_4, 30 SiO_2	Mn_7SiO_{12}, Mn_2O_3, SiO_2	Mn_7SiO_{12}, Mn_3O_4
MSi50	50 Mn_3O_4, 50 SiO_2	Mn_7SiO_{12}, SiO_2	Mn_7SiO_{12}, $MnSiO_3$

Table 8b. *Identified crystalline phases of Mn-Si-O materials. Particles were sintered at 1150°C.The main phases were presented first followed by minor phases.*

Notation	**Raw materials** *(wt%)*	**Phases in fresh sample (calcined at 1150°C)**	**Phases in used sample**
MSi6	94 Mn_3O_4, 6 SiO_2	Mn_7SiO_{12}, Mn_2O_3	Mn_7SiO_{12}, Mn_3O_4
MSi15	85 Mn_3O_4, 15 SiO_2	Mn_7SiO_{12}	Mn_7SiO_{12}, Mn_3O_4
MSi25	75 Mn_3O_4, 25 SiO_2	Mn_7SiO_{12}	Mn_7SiO_{12}, Mn_3O_4
MSi35	65 Mn_3O_4, 35 SiO_2	Mn_7SiO_{12}, $MnSiO_3$	$MnSiO_3$, Mn_3O_4
MSi45	55 Mn_3O_4, 45 SiO_2	$MnSiO_3$, SiO_2	$MnSiO_3$, SiO_2
MSi50	50 Mn_3O_4, 50 SiO_2	$MnSiO_3$, SiO_2	$MnSiO_3$, SiO_2
MSi75	25 Mn_3O_4, 75 SiO_2	$MnSiO_3$, SiO_2, SiO_2*	$MnSiO_3$, SiO_2, SiO_2*

Note: SiO_2* is cristoballite phase SiO_2. The phase for the SiO_2 without mark is quartz phase.

Table 9. *Identified crystalline phases of Mn-Mg-O materials. The main phases were presented first followed by minor phases. The samples with same composition but sintered at different temperatures had the same crystalline phases.*

Notation	Raw materials (wt%)	Phases in fresh sample	Phases in used sample
MMg21	79.1% Mn_3O_4, 20.9% MgO	Mg_2MnO_4, $MgMn_2O_4$	$MgMn_2O_4$
MMg26	74.0% Mn_3O_4, 26.0% MgO	Mg_2MnO_4, $MgMn_2O_4$	$MgMn_2O_4$
MMg35	65.4% Mn_3O_4, 34.6% MgO	Mg_2MnO_4	Mg_2MnO_4

Table 10. *Identified crystalline phases of CuO-based materials on which reactivity tests were successfully performed. The main phases were presented first followed by minor phases.*

Notation	**Raw materials (wt%)**	**Phases in fresh sample**	**Phases in used sample**
Cu40Z-950	40 CuO, 60 ZrO_2	CuO, ZrO_2	CuO, ZrO_2
Cu40ZLa5-950	40 CuO, 55 ZrO_2, 5 La_2O_3	CuO, ZrO_2, $La_2Zr_2O_7$	CuO, ZrO_2, $La_2Zr_2O_7$
Cu40(YSZ)-1100	40 CuO, 60 YSZ	CuO, $Zr_xY_{1-x}O_2$	CuO, $Zr_xY_{1-x}O_2$
Cu40Ce-950	40 CuO, 60 CeO_2	CuO, CeO_2	CuO, CeO_2
Cu40(MgAl)-1100	40 CuO, 60 $MgAl_2O_4$	CuO, $MgAl_2O_4$	CuO, $MgAl_2O_4$
Cu40(MgAl*)-1100	40 CuO, 60$MgAl_2O_4$*	CuO, $MgAl_2O_4$	CuO, $MgAl_2O_4$
Cu40(MgAl)La5-1100	40 CuO, 60 $MgAl_2O_4$, 5 La_2O_3	CuO, $MgAl_2O_4$, $LaAlO_3$	CuO, $MgAl_2O_4$, $LaAlO_3$
Cu60F-950	60 CuO, 40 Fe_2O_3	CuO, $Cu_xFe_{3-x}O_4$	CuO, $Cu_xFe_{3-x}O_4$
Cu40MgF48-950	40 CuO, 48 Fe_2O_3, 12 MgO	CuO, $MgFe_2O_4$	CuO, $MgFe_2O_4$
Cu36FAl24-1100	36 CuO, 40 Fe_2O_3, 24 Al_2O_3	$Cu_{0.95}Fe_{1.05}AlO_4$	$Cu_{0.95}Fe_{1.05}AlO_4$

3.5 Rate index and solid inventory

In this work a large number of oxygen carrier materials have been investigated, with a certain focus on combined manganese oxides, including the perovskite system $CaMn_yX_{1-y}O_{3-\delta}$ (Paper II-V), Mn-Si (Paper VI), Mn-Fe-Si (Paper I), Mn-Mg-O (Paper I) in addition to several ternary compositions (Paper I). It would be of interest to compare the performance of these in a coherent manner. In Paper V, two pseudo first-order rate constants were used to evaluate results for the perovskite system $CaMn_{0.775}Mg_{0.1}Ti_{0.125}O_3$. In the following section, the rate index (RI) is used to compare the reactivity of some of the more interesting materials investigated in this work, see Paper V for details. A rate index, RI, is defined in equation 17 as:

$$\text{Rate index (RI)} = 60 \cdot 100 \cdot \left(\frac{d\omega}{dt} \right)_{norm} \tag{17}$$

The normalized rate of solid conversion of oxygen carrier is calculated from a pseudo-first order effective rate constant, k'_{eff}, and an average partial pressure of methane,

$$\left(\frac{d\omega}{dt} \right)_{norm} = k'_{eff}(\omega)\, p_{ref} \tag{18}$$

where p_{ref} is a reference partial pressure of methane, here chosen to be 0.15, which would approximately correspond to a full conversion of the gas [112]. The effective rate constant k'_{eff} was calculated from the fluidized bed experiments, according to the procedure outlined in Paper V. In Figure 25, the RI is shown as a function of the crushing strength (N) for several systems investigated in this work, which have shown promise with respect to reactivity, oxygen uncoupling and stability. The corresponding solids inventory needed in the fuel reactor is also shown. Here each set of oxygen carrier represents one promising composition or stoichiometry. As some compositions were calcined at different temperatures, these are included as well. The sintering temperature was an important parameter to vary in order to increase strength and stability, and often spray-dried materials in this work were sintered at a minimum of two temperatures. The rate index was evaluated at two specific values of the mass based conversion, ω=0.997 and ω=0.99. There is a clear decrease in reactivity as the degree of oxidation decreases.

The rate index varied in a wide range, but there were several systems which displayed a combination of high reactivity and high CS, i.e. >2 N. The rate index is the normalized conversion rate expressed in percentage mass change per minute. Thus, the needed mass of bed material needed in the fuel reactor is proportional to the rate index, under the assumption for which the normalized conversion rate was derived. These are: i) the fuel is methane, ii) the reaction is first order with respect to methane and iii) the mass transfer resistance between the bubble phase and dense phase is small. As all oxygen carriers in the figure release oxygen to the gas phase via CLOU, it is likely that the fuel is converted via several mechanisms, and thus it is not likely that the reaction order is unity. Further, the last assumption is not necessarily true and is very dependent on the fluidizing conditions. Thus, the needed bed mass can be calculated by utilizing the methodology outlined by Mattisson et al., according to which a rate index of 5 would correspond to a bed mass of 100 kg/MW_{th} [20]. From Figure 25, it is clear that most of

the oxides here theoretically need very little solids inventory to achieve full gas yield to CO_2. It is desirable to minimize the amount of bed material in the reactors: this will reduce the size and investment cost of the system and also mean that less power will be needed by the fans which supply the reacting gas to the reactors.

The oxygen carriers shown in Figure 25 have been tested in continuous operation in CLC units ranging from 0.3-120 kW using natural gas as fuel in the temperature range 900-960°C, see a review of these results by Mattisson et al. [92]. Although the specific solids inventory was higher than those predicted in Figure 25, full gas conversion to CO_2 could be obtained for the $CaMn_{0.9}Mg_{0.1}O_{3-\delta}$ in units from 0.3-120 kW. Similar results have been obtained for the reference material $CaMn_{0.775}Mg_{0.1}Ti_{0.125}O_{3-\delta}$ in Paper V. With respect to $(Mn_{0.66}Fe_{0.33})_2SiO_3$ Källén et al. was able to achieve full gas yield at 235 kg/MW oxygen carrier using a continuous bench-scale reactor [113]. The MnSi25 material has also been tested by Källén et al., and here full gas yield was obtained already using 150 kg/MW, although major problems with attrition was found [114]. Similar problems were seen with the $MnMgO_x$ material, although up to 93% methane conversion was seen in a bench-scale reactor [92].

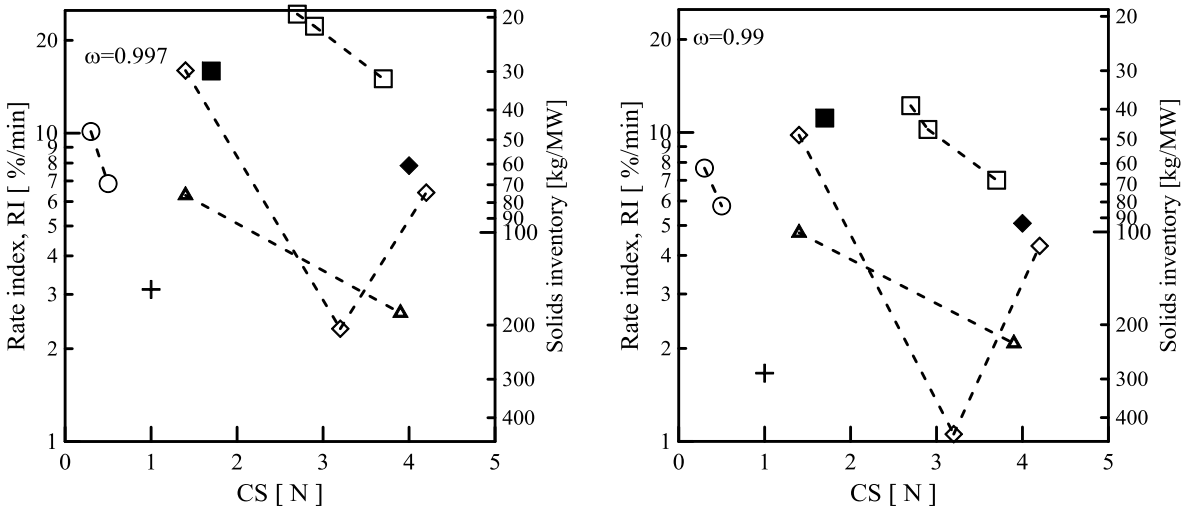

Figure 25. The RI as a function of CS for several system investigated in this work, evaluated at two levels of the mass-based conversion: ω=0.997 (a) and 0.99 (b). All materials were evaluated with CH_4 at 950°C. Materials are as follows: (◇) $CaMn_{0.9}Mg_{0.1}O_{3-\delta}$ (Paper II), (□) $CaMn_{0.775}Mg_{0.1}Ti_{0.125}O_{3-\delta}$ (Paper V), (○) Mn-Si (Paper VI), (▵) $MnMgO_X$ (Paper I), (+) $(Mn_{0.66}Fe_{0.33})_2SiO_3$ (Paper I)

4 Discussion

Prior to the start of this work, oxygen carriers that had been examined were mainly pure metal oxides, for instance Fe_2O_3 [47, 98, 115], CuO [25, 104], Mn_3O_4 [67, 112] and NiO [26, 53, 63]. Among the investigated CLC materials, NiO presented very high reactivity towards CH_4 and had an estimated lifetime over 30 000 h [63]. With respect to CLOU, not so much had been performed, and CuO was the most studied materials [14, 116]. For NiO, there are obvious disadvantages, although it was the state-of-art material for gas CLC application. The biggest drawbacks with Ni are that it is expensive and toxic. Additionally, NiO has thermodynamic limitation for conversion of hydrocarbons to carbon dioxide. Hence, it is not possible to achieve 100% conversion of CH_4 to CO_2 and H_2O neither in a batch fluidized reactor nor in continuous units [26, 63]. On the other hand, CuO has sufficient equilibrium oxygen partial pressure and fast oxygen releasing kinetics under combustion conditions to be highly relevant for CLOU [14]. But the agglomeration and attrition problems reported in the literature are drawbacks [39, 75, 76] . To take CLC to the next level of development with proper oxygen carriers, the theme of this work was to investigate non-Ni containing oxygen carriers which are cheap, environmentally friendly and have the ability to fully convert CH_4 to CO_2 and H_2O. As it is believed that materials with some CLOU properties have advantages for achieving this, the focus has been on such materials. Although the main effort is on the so-called combined manganese oxides, CuO with new and innovative support materials is also a part of the thesis work.

A combined oxide, as used in this work, is a combination of Mn with other elements to overcome the thermodynamic and kinetic disadvantage of pure manganese oxide. In this work several binary and ternary systems have been investigated with respect to application to CLOU. Systems with great promise include Ca-Mn-X-O (X=Fe, Ti and Mg), Mn-Si-O and Mn-Mg-O. Particles of the different systems were produced by the commercial industrial process spray-drying. The choice of combined oxygen carrier system was derived not only from thermodynamic calculations, but also from price of raw materials and environmental aspects, e.g. no nickel was employed in any of the investigated materials.

Some of the materials examined clearly have great promise. For instance, the perovskite $CaMnO_{3-\delta}$ can fully convert CH_4 to CO_2 and H_2O. While at the same experimental conditions, NiO reached maximum of 99% [26]. In a 10 kW continuous unit operated at gas velocities similar to what would be expected in an industrial plant, full conversion of CH_4 was achieved for this type of material [93]. Both of the $CaMn_{0.9}Mg_{0.1}O_{3-\delta}$ and $CaMn_{0.775}Mg_{0.1}Ti_{0.125}O_{3-\delta}$ oxygen carriers were also examined in a 120 kW continuous unit using gaseous fuels. The oxygen carriers can achieve 100% CH_4 conversion at a temperature of 950ºC-965ºC with a solid inventory 320-350 kg/MW. At certain conditions, oxygen was also found in the outlet stream from the fuel reactor, which can be attributed to the CLOU effect [92].

This should be compared to when NiO was tested in continuous unit, where about 1% CO and 0.5% unconverted CH_4 were detected after the fuel reactor [64]. The calcium manganite oxygen carrier was also successfully applied for liquid and solid fuel including biomass combustion in lab scale continuous CLC unit [103, 117, 118]. Although more thorough examinations need to

be performed, $CaMnO_{3-\delta}$ seems to have comparable or better performance compared to Ni-based oxygen carriers. The fact that the material can be produced with low cost and environmentally friendly raw powders is certainly an advantage. In the thesis, a major effort was also undertaken to produce the $CaMnMgTiO_{3-\delta}$ oxygen carrier with materials actually available on the market at multi-ton scale. Titanium was included into the structure, as it was found that this could have a stabilizing effect and prevent deactivation, which could occur with the undoped material. From this study it is quite clear that the oxygen carrier is very simple to produce. With the spray-dried compositions evaluated (50.3 wt% $Ca(OH)_2$, 40.1 wt% Mn_3O_4, 2.7 wt% MgO and 6.8 wt% TiO_2), all resulted in perovskite formation. All oxygen carriers showed the characteristic oxygen release pattern expected from perovskites, given varied reactivities.

In addition to the calcium manganites, there are a number of other interesting combined oxides developed in this work. The system of Mn-Si-O materials showed high reactivity with methane and a very high CLOU activity at higher temperatures. Also, these oxygen carriers are produced with relatively cheap and benign raw materials. Besides Mn_3O_4, the other raw material of these oxygen carriers was SiO_2 which is the main constituent in sand. Further, the third system of considerable interest is the Mn-Mg-O combined oxides. $MnMgO_x$ released considerable gaseous oxygen and converted about 90% CH_4 under the current experimental conditions. The material had a similar oxygen release mechanism as for the perovskite material, but unfortunately major problems with agglomeration were detected when this material was tested in a bench-scale continuous CLC reactor. It would be of interest to try and optimize and improve performance of such a material. With respect to the work done on combined manganese oxides, this thesis presents a large part of the work done up to date, see Paper I. Not only have a number of materials been produced which are ready for up-scaling to tonnage scale, but also several systems have been identified having clear potential, but may need further optimization with respect to stability and strength.

Finally, some work was also undertaken with Cu-based oxygen carriers. Some of the support materials, for instance $CuFe_2O_4$ and $MgFe_2O_4$, which had not been examined on CuO previously, were investigated in this work. Except for the material utilizing the combined Fe_2O_3, Al_2O_3 support, the rest of the supports worked well with CuO in the batch fluidized bed reactor. Full CH_4 conversion with high oxygen released were observed. Neither agglomeration nor attrition was noticed in the batch fluidized experiments. However, the CuO oxygen carriers suffered from physical integration during continuous testing in the Chalmers 300 W_{th} CLC unit.

5 Conclusion

In this work, four innovative oxygen-carrier systems were investigated, i.e. Ca-Mn-X-O (X=Cu, Fe, Ti and Mg) oxygen carriers with perovskite structure, the Mn-Si-O system, material based on Mn-Mg-O and finally CuO-based materials. All of these non-Ni materials were manufactured by spray-drying and examined with respect to parameters important for chemical-looping. The main conclusions are:

- In the Ca-Mn-X-O (X=Fe, Ti and Mg) system, all these perovskite materials performed very well. By increase the operational temperature from 900ºC to 950ºC, the reactivity of the studied perovskite material can be obviously improved. Adjustment of production parameters, i.e. calcination temperature, calcination time and milling time, can be useful for the optimization of oxygen carrier's properties. Raw materials available in tonnage scale, such as Mn-oxide and TiO_2 sources, are feasible to produce perovskite $CaMnO_{3-\delta}$ type oxygen carrier with high performance. These perovskite materials presented better reactivity towards CH_4 in both batch fluidized reactor and continuous unit, also with the advantage of cost and environmental friendly, it could be an alternative to the benchmark NiO oxygen carrier.

- Although the oxygen carriers based on Mn-Si-O had limited oxygen release at lower temperatures, there was a remarkable increase in release at temperatures above 950°C for particles with less than 45 wt% SiO_2. Similarly, the ability to convert CH_4 for these particles increased with temperature, and over 90% combustion could be achieved at temperatures at and above 950°C.

- The final combined oxide system investigated was a combination of the cations Mn and Mg. In contrast to the Mn and Si system, the uncoupling reactions were more pronounced at 900°C, and also the methane conversion for some particles investigated was high, making this yet another interesting alternative.

- CuO-based materials with different support materials have a seemingly fast release rate of oxygen, approaching equilibrium at 900°C. Further, most investigated materials had the ability to fully convert CH_4 at 925°C at the experimental conditions employed here. Some Cu-support combinations did not perform so well, for instance the Cu36FAl24 sample did not have very promising reactivity due to formation of $Cu_{0.95}Fe_{1.05}AlO_4$.

6 References

[1] International Energy Agency Agency I. E. (2013), CO_2 Emissions from Fuel Combustion *Highlights* (2012 Edition)

[2] Cox P. M., Betts R. A., Jones C. D., Spall S. A.,Totterdell I. J. (2000), Acceleration of global warming due to carbon-cycle feedbacks in a coupled climate model, Nature 6809(408), pp. 184-187

[3] Metz B., Davidson O., de Coninck H. C., Loos M.,Meyer L. A. (2005), IPCC Special Report on Carbon Dioxide Capture and Storage. Prepared by Working Group III of the Intergovernmental Panel on Climate Change, Journal pp.

[4] Global Carbon Capture and Storage Institute (2012), CO2 capture technologies: Pre-Combustion Capture

[5] Scholes C. A., Smith K. H., Kentish S. E.,Stevens G. W. (2010), CO2 capture from pre-combustion processes—Strategies for membrane gas separation, International Journal of Greenhouse Gas Control 5(4), pp. 739-755

[6] Wang M., Lawal A., Stephenson P., Sidders J.,Ramshaw C. (2011), Post-combustion CO2 capture with chemical absorption: A state-of-the-art review, Chemical Engineering Research and Design 9(89), pp. 1609-1624

[7] Toftegaard M. B., Brix J., Jensen P. A., Glarborg P.,Jensen A. D. (2010), Oxy-fuel combustion of solid fuels, Progress in Energy and Combustion Science 5(36), pp. 581-625

[8] Ishida M.,Jin H. (1996), A Novel Chemical-Looping Combustor without NOx Formation, Industrial & Engineering Chemistry Research 7(35), pp. 2469-2472

[9] Lyngfelt A., Leckner B.,Mattisson T. (2001), A fluidized-bed combustion process with inherent CO2 separation; application of chemical-looping combustion, Chemical Engineering Science 10(56), pp. 3101-3113

[10] Kronberger B., Johansson E., Loeffler G., Mattisson T., Lyngfelt A.,Hofbauer H. (2004), A two-compartment fluidized bed reactor for CO_2 capture by chemical-looping combustion, Chemical Engineering & Technology 12(27), pp. 1318-1326

[11] Mattisson T., Lyngfelt A.,Leion H. (2009), Chemical-looping with oxygen uncoupling for combustion of solid fuels, International Journal of Greenhouse Gas Control 1(3), pp. 11-19

[12] Mattisson T., Leion H.,Lyngfelt A. (2009), Chemical-looping with oxygen uncoupling using CuO/ZrO_2 with petroleum coke, Fuel 4(88), pp. 683-690

[13] Leion H., Mattisson T.,Lyngfelt A. (2009), Using chemical-looping with oxygen uncoupling (CLOU) for combustion of six different solid fuels, Greenhouse Gas Control Technologies 9 Issue, pp. 447-453

[14] Mattisson T. (2013), Materials for Chemical-Looping with Oxygen Uncoupling, ISRN Chemical Engineering 2013), pp. 19 pages

[15] Gayan P., Forero C. R., Abad A., de Diego L. F., Garcia-Labiano F.,Adanez J. (2011), Effect of Support on the Behavior of Cu-Based Oxygen Carriers during Long-Term CLC Operation at Temperatures above 1073 K, Energy & Fuels 3(25), pp. 1316-1326

[16] Baek J.-I., Kim J.-W., Lee J. B., Eom T. H., Ryu J., Ryu C. K.,Yi J. (2011), Effects of Support on the Performance of NiO-Based Oxygen Carriers, Oil Gas Sci. Technol. – Rev. IFP Energies nouvelles 2(66), pp. 223-234

[17] Gayán P., de Diego L. F., García-Labiano F., Adánez J., Abad A.,Dueso C. (2008), Effect of support on reactivity and selectivity of Ni-based oxygen carriers for chemical-looping combustion, Fuel 12(87), pp. 2641-2650

[18] Acres G. J. K., Bird A. J., Jenkins J. W.,King F. (1981), The design and preparation of supported catalysts, Catalysis: Volume 4 Issue, pp. 1-30

[19] Hedayati A., Azad A.-M., Rydén M., Leion H.,Mattisson T. (2012), Evaluation of Novel Ceria-Supported Metal Oxides As Oxygen Carriers for Chemical-Looping Combustion, Industrial & Engineering Chemistry Research 39(51), pp. 12796-12806

[20] Mattisson T., Johansson M.,Lyngfelt A. (2004), Multicycle Reduction and Oxidation of Different Types of Iron Oxide Particles-Application to Chemical-Looping Combustion, Energy & Fuels 3(18), pp. 628-637

[21] Arjmand M., Azad A. M., Leion H., Lyngfelt A.,Mattisson T. (2011), Prospects of Al2O3 and MgAl2O4-Supported CuO Oxygen Carriers in Chemical-Looping Combustion (CLC) and Chemical-Looping with Oxygen Uncoupling (CLOU), Energy & Fuels 11(25), pp. 5493-5502

[22] Dong W.-S., Jun K.-W., Roh H.-S., Liu Z.-W.,Park S.-E. (2002), Comparative study on partial oxidation of methane over Ni/ZrO_2, Ni/CeO_2 and $Ni/Ce\text{-}ZrO_2$ catalysts, Catalysis Letters 1-4(78), pp. 215-222

[23] Johansson M., Mattisson T.,Lyngfelt A. (2006), Investigation of Mn_3O_4 with stabilized ZrO_2 for chemical-looping combustion, Chemical Engineering Research and Design A9(84), pp. 807-818

[24] Galinsky N. L., Huang Y., Shafiefarhood A.,Li F. (2013), Iron Oxide with Facilitated O2 − Transport for Facile Fuel Oxidation and CO2 Capture in a Chemical Looping Scheme, ACS Sustainable Chemistry & Engineering 3(1), pp. 364-373

[25] Chuang S. Y., Dennis J. S., Hayhurst A. N.,Scott S. A. (2008), Development and performance of Cu-based oxygen carriers for chemical-looping combustion, Combustion and Flame 1-2(154), pp. 109-121

[26] Jerndal E., Mattisson T.,Lyngfelt A. (2009), Investigation of Different NiO/NiAl2O4 Particles as Oxygen Carriers for Chemical-Looping Combustion, Energy & Fuels 1(23), pp. 665-676

[27] Azad A. M., Hedayati A., Rydén M., Leion H.,Mattisson T. (2013), Examining the Cu − Mn − O Spinel System as an Oxygen Carrier in Chemical Looping Combustion, Energy Technology 1(1), pp. 59-69

[28] Azimi G., Leion H., Rydén M., Mattisson T.,Lyngfelt A. (2012), Investigation of Different Mn − Fe Oxides as Oxygen Carrier for Chemical-Looping with Oxygen Uncoupling (CLOU), Energy & Fuels 1(27), pp. 367-377

[29] Jerndal E., Mattisson T.,Lyngfelt A. (2006), Thermal analysis of chemical-looping combustion, Chemical Engineering Research and Design A9(84), pp. 795-806

[30] Jin H., Okamoto T.,Ishida M. (1999), Development of a Novel Chemical-Looping Combustion: Synthesis of a Solid Looping Material of $NiO/NiAl_2O_4$, Industrial & Engineering Chemistry Research 1(38), pp. 126-132

[31] Lee J.-B., Song Y.-W., Park C.-S., Choi S.-I., Kim Y.-H.,Yang H.-S. (2003), Redox reaction characteristics of metal oxide mediums for chemical-looping combustion, Nonmunjip - Ch'ungnam Taehakkyo Sanop Kisul Yon'guso 2(18), pp. 83-91

[32] Mattisson T., Jaerdnaes A.,Lyngfelt A. (2003), Reactivity of Some Metal Oxides Supported on Alumina with Alternating Methane and Oxygen-Application for Chemical-Looping Combustion, Energy & Fuels 3(17), pp. 643-651

[33] Jeong J. H., Park J. W.,Yoon W. L. (2003), Redox characteristics of $CoOx/CoAl_2O_4$ as a oxygen carrier for chemical-looping combustion, Kongop Hwahak 4(14), pp. 411-417

[34] Jin H., Okamoto T.,Ishida M. (1998), Development of a Novel Chemical-Looping Combustion: Synthesis of a Looping Material with a Double Metal Oxide of CoO-NiO, Energy & Fuels 6(12), pp. 1272-1277

[35] Ryu H.-J., Jin G.-T., Bae D.-H.,Yi C.-K. (2004), Continuous Operation of a 50kWth Chemical-Looping Combustor: Long-Term Operation with Ni- and Co-Based Oxygen Carrier Particles, Presented at the 5th China-Korea Joint Workshop on Clean Energy Technology, October 25-28, Qingdao University, China, 2004 pp. 221-230

[36] Roux S., Bensakhria A.,Antonini G. (2006), Study and improvement of the regeneration of metallic oxides used as oxygen carriers for a new combustion process, International Journal of Chemical Reactor Engineering 4), pp. No pp given

[37] Son S. R.,Kim S. D. (2006), Chemical-Looping Combustion with NiO and Fe2O3 in a Thermobalance and Circulating Fluidized Bed Reactor with Double Loops, Industrial & Engineering Chemistry Research 8(45), pp. 2689-2696

[38] Shen L., Wu J., Xiao J., Song Q.,Xiao R. (2009), Chemical-Looping Combustion of Biomass in a 10 kWth Reactor with Iron Oxide As an Oxygen Carrier, Energy & Fuels 5(23), pp. 2498 − 2505

[39] Cho P., Mattisson T.,Lyngfelt A. (2004), Comparison of iron-, nickel-, copper- and manganese-based oxygen carriers for chemical-looping combustion, Fuel 9(83), pp. 1215-1225

[40] Lambert A., Delquié C., Clémeneçon I., Comte E., Lefebvre V., Rousseau J.,Durand B. (2009), Synthesis and characterization of bimetallic Fe/Mn oxides for chemical looping combustion, Energy Procedia 1(1), pp. 375-381

[41] Ishida M.,Jin H. (1997), CO_2 recovery in a power plant with chemical looping combustion, Energy Conversion and Management Suppl., Proceedings of the Third International Conference on Carbon Dioxide Removal, 1996(38), pp. S187-S192

[42] Li F., Luo S., Sun Z., Bao X.,Fan L. S. (2011), Role of metal oxide support in redox reactions of iron oxide for chemical looping applications: Experiments and density functional theory calculations, Energy and Environmental Science 9(4), pp. 3661-3667

[43] Brown T. A., Dennis J. S., Scott S. A., Davidson J. F.,N. H. A. (2010), Gasification and Chemical-Looping Combustion of a Lignite Char in a Fluidized Bed of Iron Oxide, Energy & Fuels 24), pp. 3034-3048

[44] Leion H., Jerndal E., Steenari B. M., Hermansson S., Israelsson M., Jansson E., Johnsson M., Thunberg R., AVadenbo A., Mattisson T.,Lyngfelt A. (2009), Solid fuels in chemical-looping combustion using oxide scale and unprocessed iron ore as oxygen carriers, Fuel 10(88), pp. 1945 − 1954

[45] Wang B., Zhao H., Zheng Y., Liu Z., Yan R.,Zheng C. (2012), Chemical looping combustion of a Chinese anthracite with Fe2O3-based and CuO-based oxygen carriers, Fuel Processing Technology 0(96), pp. 104-115

[46] Abad A., Adanez J., Garcia-Labiano F., De Diego L. F., Gayan P.,Celaya J. (2007), Mapping of the range of operational conditions for Cu-, Fe-, and Ni-based oxygen carriers in chemical-looping combustion, Chemical Engineering Science 1-2(62), pp. 533-549

[47] Adanez J., de Diego L. F., Garcia-Labiano F., Gayan P., Abad A.,Palacios J. M. (2004), Selection of Oxygen Carriers for Chemical-Looping Combustion, Energy & Fuels 2(18), pp. 371-377

[48] Johansson M., Mattisson T.,Lyngfelt A. (2004), Investigation of Fe_2O_3 with $MgAl_2O_4$ for Chemical-Looping Combustion, Industrial & Engineering Chemistry Research 22(43), pp. 6978-6987

[49] Adanez J., Abad A., Garcia-Labiano F., Gayan P.,De Diego L. F. (2012), Progress in chemical-looping combustion and reforming technologies, Progress in Energy and Combustion Science 2(38), pp. 215-282

[50] Quddus M. R., Hossain M. M.,de Lasa H. I. (2013), Ni based oxygen carrier over γ -Al2O3 for chemical looping combustion: Effect of preparation method on metal support interaction, Catalysis Today 0(210), pp. 124-134

[51] Mattisson T., Jerndal E., Linderholm C.,Lyngfelt A. (2011), Reactivity of a spray-dried NiO/NiAl2O4 oxygen carrier for chemical-looping combustion, Chemical Engineering Science 20(66), pp. 4636-4644

[52] Jerndal E., Mattisson T., Thijs I., Snijkers F.,Lyngfelt A. (2010), Investigation of NiO/NiAl2O4 oxygen carriers for chemical-looping combustion produced by spray-drying, International Journal of Greenhouse Gas Control 1(4), pp. 23-35

[53] Shen L., Wu J.,Xiao J. (2009), Experiments on chemical looping combustion of coal with a NiO based oxygen carrier, Combustion and Flame 156), pp. 721-728

[54] Leion H., Mattisson T.,Lyngfelt A. (2009), Solid fuels in chemical-looping combustion using a NiO-based oxygen carrier, Chemical Engineering Research and Design 1943-1550), pp.

[55] Shulman A., Linderholm C., Mattisson T.,Lyngfelt A. (2009), High Reactivity and Mechanical Durability of NiO/NiAl2O4 and NiO/NiAl2O4/MgAl2O4 Oxygen Carrier Particles Used for more than 1000 h in a 10 kW CLC Reactor, Industrial & Engineering Chemistry Research 15(48), pp. 7400-7405

[56] Bolhar-Nordenkampf J., Proll T., Kolbitsch P.,Hofbauer H. (2009), Performance of a NiO-based oxygen carrier for chemical looping combustion and reforming in a 120kW unit, Greenhouse Gas Control Technologies 9 1(1), pp. 19-25

[57] Hoteit A., Chandel M. K.,Delebarre A. (2009), Nickel- and Copper-Based Oxygen Carriers for Chemical Looping Combustion, Chemical Engineering & Technology 3(32), pp. 443-449

[58] Zhao H., Liu L., Wang B., Xu D., Jiang L.,Zheng C. (2008), Sol − Gel-Derived NiO/NiAl2O4 Oxygen Carriers for Chemical-Looping Combustion by Coal Char, Energy & Fuels 2(22), pp. 898 − 905

[59] Siriwardane R., Poston J., Chaudhari K., Zinn A., Simonyi T.,Robinson C. (2007), Chemical-Looping Combustion of Simulated Synthesis Gas Using Nickel Oxide Oxygen Carrier Supported on Bentonite, Energy & Fuels 3(21), pp. 1582-1591

[60] Liu T., Simonyi T., Sanders T., Siriwardane R.,Veser G. (2007), Comparative evaluation of Ni-, Cu-, and Fe-based oxygen carriers for chemical looping combustion, Abstracts of Papers, 233rd ACS National Meeting, Chicago, IL, United States, March 25-29, 2007 pp. INOR-723

[61] Zafar Q., Abad A., Mattisson T.,Gevert B. (2007), Reaction Kinetics of Freeze-Granulated $NiO/MgAl_2O_4$ Oxygen Carrier Particles for Chemical-Looping Combustion, Energy & Fuels 2(21), pp. 610-618

[62] Mattisson T., Johansson M.,Lyngfelt A. (2006), The use of NiO as an oxygen carrier in chemical-looping combustion, Fuel 5-6(85), pp. 736-747

[63] Linderholm C., Mattisson T.,Lyngfelt A. (2009), Long-term integrity testing of spray-dried particles in a 10 kW chemical-looping combustor using natural gas as fuel, Fuel 88), pp. 2083-2096

[64] Linderholm C., Abad A., Mattisson T.,Lyngfelt A. (2008), 160 hours of chemical-looping combustion in a 10 kW reactor system with a NiO-based oxygen carrier, International Journal of Greenhouse Gas Control 4(2), pp. 520-530

[65] Kolbitsch P., Bolhar-Nordenkampf J., Proll T.,Hofbauer H. (2010), Operating experience with chemical looping combustion in a 120 kW dual circulating fluidized bed (DCFB) unit, International Journal of Greenhouse Gas Control 2(4), pp. 180-185

[66] Johansson M., Mattisson T.,Lyngfelt A. (2006), Use of $NiO/NiAl_2O_4$ Particles in a 10 kW Chemical-Looping Combustor, Industrial & Engineering Chemistry Research 17(45), pp. 5911-5919

[67] Zafar Q., Abad A., Mattisson T., Gevert B.,Strand M. (2007), Reduction and oxidation kinetics of Mn3O4/Mg − ZrO2 oxygen carrier particles for chemical-looping combustion, Chemical Engineering Science 23(62), pp. 6556-6567

[68] Forero C. R., Gayán P., García-Labiano F., de Diego L. F., Abad A.,Adánez J. (2011), High temperature behaviour of a CuO/ γ Al2O3 oxygen carrier for chemical-looping combustion, International Journal of Greenhouse Gas Control 4(5), pp. 659-667

[69] Wang S., Luo M., Wang G., Wang L.,Lv M. (2012), Analysis of Reactivity of a CuO-Based Oxygen Carrier for Chemical Looping Combustion of Coal, Energy & Fuels 6(26), pp. 3275-3283

[70] Gayan P., Adanez-Rubio I., Abad A., De Diego L. F., Garcia-Labiano F.,Adanez J. (2012), Development of Cu-based oxygen carriers for Chemical-Looping with Oxygen Uncoupling (CLOU) process, Fuel 1(96), pp. 226-238

[71] Adanez-Rubio I., Gayan P., Abad A., De Diego L. F., Garcia-Labiano F.,Adanez J. (2012), Evaluation of a Spray-Dried CuO/MgAl2O4 Oxygen Carrier for the Chemical Looping with Oxygen Uncoupling Process, Energy & Fuels 5(26), pp. 3069-3081

[72] de Diego L. F., Garcia-Labiano F., Adanez J., Gayan P., Abad A., Corbella B. M.,Palacios J. M. (2004), Development of Cu-based oxygen carriers for chemical-looping combustion, Fuel 13(83), pp. 1749-1757

[73] Imtiaz Q., Kierzkowska A. M.,Müller C. R. (2012), Coprecipitated, Copper-Based, Alumina-Stabilized Materials for Carbon Dioxide Capture by Chemical Looping Combustion, ChemSusChem 8(5), pp. 1610-1618

[74] Kierzkowska A. M.,Müller C. R. (2013), Sol − Gel-Derived, Calcium-Based, Copper-Functionalised CO2 Sorbents for an Integrated Chemical Looping Combustion − Calcium Looping CO2 Capture Process, ChemPlusChem 1(78), pp. 92-100

[75] De Diego L. F., Gayan P., Garcia-Labiano F., Celaya J., Abad A.,Adanez J. (2005), Impregnated CuO/Al_2O_3 Oxygen Carriers for Chemical-Looping Combustion: Avoiding Fluidized Bed Agglomeration, Energy & Fuels 5(19), pp. 1850-1856

[76] Copeland J. R., Alptekin G., Cesaria M.,Gershkovich Y. (2002), Sorbent Energy Transfer System (SETS) for CO_2 Separation With High Efficiency, 27th International Conference on Coal Utilization & Fuel Systems, Clearwater, USA

[77] Arjmand M., Azad A.-M., Leion H., Mattisson T.,Lyngfelt A. (2012), Evaluation of CuAl2O4 as an Oxygen Carrier in Chemical-Looping Combustion, Industrial & Engineering Chemistry Research 43(51), pp. 13924-13934

[78] Shulman A., Cleverstam E., Mattisson T.,Lyngfelt A. (2011), Chemical - Looping with oxygen uncoupling using Mn/Mg-based oxygen carriers - Oxygen release and reactivity with methane, Fuel 3(90), pp. 941-950

[79] Kjellqvist L.,Selleby M. (2010), Thermodynamic assessment of the Fe-Mn-O system, Jornal of Phase Equilibria and Diffusion 2(31), pp. 113-134

[80] Johansson M., Mattisson T.,Lyngfelt A. (2006), Creating a Synergy Effect by Using Mixed Oxides of Iron- and Nickel Oxides in the Combustion of Methane in a Chemical-Looping Combustion Reactor, Energy & Fuels 6(20), pp. 2399-2407

[81] Azimi G., Mattisson T., Leion H., Rydén M.,Lyngfelt A. (2015), Comprehensive study of Mn − Fe − Al oxygen-carriers for chemical-looping with oxygen uncoupling (CLOU), International Journal of Greenhouse Gas Control 0(34), pp. 12-24

[82] Arjmand M., Frick V., Rydén M., Leion H., Mattisson T.,Lyngfelt A. (2015), Screening of Combined Mn-Fe-Si Oxygen Carriers for Chemical Looping with Oxygen Uncoupling (CLOU), Energy & Fuels 3(29), pp. 1868-1880

[83] Rydén M., Leion H., Mattisson T.,Lyngfelt A. (2014), Combined oxides as oxygen-carrier material for chemical-looping with oxygen uncoupling, Applied Energy 0(113), pp. 1924-1932

[84] Azimi G., Rydén M., Leion H., Mattisson T.,Lyngfelt A. (2013), $(Mn_zFe_{1-z})_yO_x$ combined oxides as oxygen carrier for chemical-looping with oxygen uncoupling, AIChE Journal 2(59), pp. 582-588

[85] Azimi G., Leion H., Mattisson T.,Lyngfelt A. (2010), Chemical-looping with oxygen uncoupling for Mn-based materials, testing in batch fluidized bed, 10th International Conference on Greenhouse Gas Control Technologies, 19-23 September, Amsterdam, The Netherlands

[86] Rydén M., Lyngfelt A.,Mattisson T. (2011), Combined manganese/iron oxides as oxygen carrier for chemical looping combustion with oxygen uncoupling (CLOU) in a circulating fluidized bed reactor system, Energy Procedia 0(4), pp. 341-348

[87] Shulman A., Cleverstam E., Mattisson T.,Lyngfelt A. (2009), Manganese/Iron, Manganese/Nickel, and Manganese/Silicon Oxides Used in Chemical-Looping With Oxygen Uncoupling (CLOU) for Combustion of Methane, Energy & Fuels 23), pp. 5269-5275

[88] Ksepko E., Siriwardane R. V., Tian H., Simonyi T.,Sciazko M. (2012), Effect of H2S on Chemical Looping Combustion of Coal-Derived Synthesis Gas over Fe − Mn Oxides Supported on Sepiolite, ZrO2, and Al2O3, Energy & Fuels 4(26), pp. 2461-2472

[89] Leion H., Larring Y., Bakken E., Bredesen R., Mattisson T.,Lyngfelt A. (2009), Use of $CaMn_{0.875}Ti_{0.125}O_3$ as Oxygen Carrier in Chemical-Looping with Oxygen Uncoupling, Energy & Fuels 23), pp. 5276-5283

[90] Sundqvist S., Leion H., Rydén M., Lyngfelt A.,Mattisson T. (2013), CaMn0.875Ti0.125O3− δ as an Oxygen Carrier for Chemical-Looping with Oxygen Uncoupling (CLOU)—Solid-Fuel Testing and Sulfur Interaction, Energy Technology 5-6(1), pp. 338-344

[91] Rydén M., Lyngfelt A.,Mattisson T. (2011), $CaMn_{0.875}Ti_{0.125}O_3$ as oxygen carrier for chemical-looping combustion with oxygen uncoupling (CLOU) – experiments in continuously operating fluidized bed reactor system, International Journal of Greenhouse Gas Control 2(5), pp. 356-366

[92] Mattisson T., Adánez J., Mayer K., Snijkers F., Williams G., Wesker E., Bertsch O.,Lyngfelt A. (2014), Innovative Oxygen Carriers Uplifting Chemical-looping Combustion, Energy Procedia 0(63), pp. 113-130

[93] Källén M., Rydén M., Dueso C., Mattisson T.,Lyngfelt A. (2013), CaMn0.9Mg0.1O3- δ as Oxygen Carrier in a Gas-Fired 10 kWthChemical-Looping Combustion Unit, Industrial & Engineering Chemistry Research 21(52), pp. 6923-6932

[94] Bakken E., Norby T.,Stolen S. (2005), Nonstoichiometry and reductive decomposition of CaMnO3-delta, Solid State Ionics 1-2(176), pp. 217-223

[95] Leonidova E. I., Leonidov I. A., Patrakeev M. V.,Kozhevnikov V. L. (2011), Oxygen non-stoichiometry, high-temperature properties, and phase diagram of CaMnO3-delta, Journal of Solid State Electrochemistry 5(15), pp. 1071-1075

[96] Rydén M., Leion H., Mattisson T.,Lyngfelt A. (2013), Combined oxides as oxygen-carrier material for chemical-looping with oxygen uncoupling, Applied Energy pp.

[97] Valverde-Diez N.,Grande-Fernández D. (1988), Ternary compounds of the system Mg-Mn-O as oxygen sensors, Solid State Ionics 0(28 – 30, Part 2), pp. 1697-1700

[98] Johansson M., Mattisson T.,Lyngfelt A. (2006), Comparison of Oxygen Carriers for Chemical-Looping Combustion, Thermal Science 3(10), pp. 93-107

[99] Rydén M., Moldenhauer P., Lindqvist S., Mattisson T.,Lyngfelt A. (2014), Measuring attrition resistance of oxygen carrier particles for chemical looping combustion with a customized jet cup, Powder Technology 0(256), pp. 75-86

[100] Jerndal E., Leion H., Axelsson L., Ekvall T., Hedberg M., Johansson K., Kallen M., Svensson R., Mattisson T.,Lyngfelt A. (2011), Using Low-Cost Iron-Based Materials as Oxygen Carriers for Chemical Looping Combustion, Oil & Gas Science and Technology-Revue D Ifp Energies Nouvelles 2(66), pp. 235-248

[101] Hallberg P., Källén M., Jing D., Snijkers F., van Noyen J., Rydén M.,Lyngfelt A. (2014), Experimental Investigation of $CaMnO_{3-\delta}$ Based Oxygen Carriers Used in Continuous Chemical-Looping Combustion, International Journal of Chemical Engineering 2014), pp. 9

[102] Schmitz M., Linderholm C.,Lyngfelt A. (2014), Chemical Looping Combustion of Sulphurous Solid Fuels using Calcium Manganate as Oxygen Carrier, 12th International Conference on Greenhouse Gas Control Technologies, October 5-9, Austin, Texas, USA

[103] Schmitz M., Linderholm C.,Lyngfelt A. (2014), Performance of Calcium Manganate as Oxygen Carrier in Chemical Looping Combustion of Biomass in a 10 kW pilot, 3rd International Conference on Chemical Looping, Gothenburg

[104] Adánez-Rubio I., Gayan P., Garcia-Labiano F., De Diego L. F., Adanez J.,Abad A. (2010), Development of CuO-based oxygen carrier materials suitable for Chemical-Looping with oxygen uncoupling (CLOU) process, 10th International Conference on Greenhouse Gas Control Technologies

[105] Bakken E., Boerio-Goates J., Grande T., Hovde B., Norby T., Rørmark L., Stevens R.,Stølen S. (2005), Entropy of oxidation and redox energetics of CaMnO3− δ , Solid State Ionics 29 – 30(176), pp. 2261-2267

[106] Hallberg P., Källén M., Mattisson T., Rydén M.,Lyngfelt A. (2014), Overview of operational experiences with calcium manganite oxygen carriers in chemical-looping combustion, 3rd International Conference on Chemical Looping, September 9-11, 2014, Göteborg, Sweden

[107] Imtiaz Q., Yüzbasi N. S., Kierzkowska A. M.,Müller C. R. (2012), Development of bimetallic oxygen carrier containing Fe and Cu for high syngas conversion using a modified chemical looping combustion process, International Conference on Chemical Looping, , 26-28 September 2012, Darmstadt, Germany

[108] Jacob K. T., Fitzner K.,Alcock C. B. (1977), Activities in the spinel solid solution, phase equilibria and thermodynamic properties of ternary phases in the system Cu-Fe-0, Metallurgical Transactions B 2(8), pp. 451-460

[109] Spretz R., Marchetti S. G., Ulla M. A.,Lombardo E. A. (2000), Fe/MgO Formulations for the Catalytic Combustion of Methane, Journal of Catalysis 2(194), pp. 167-174

[110] Boudart M., Delbouille A., Dumesic J. A., Khammouma S.,Topsøe H. (1975), Surface, catalytic and magnetic properties of small iron particles: I. Preparation and characterization of samples, Journal of Catalysis 3(37), pp. 486-502

[111] Topsøe H., Dumesic J. A.,Boudart M. (1973), Alumina as a textural promoter of iron synthetic ammonia catalysts, Journal of Catalysis 3(28), pp. 477-488

[112] Johansson M. (2007), Screening of oxygen-carrier particles based on iron-, manganese-, copper- and nickel oxides for use in chemical-looping technologies, Journal Issue(PhD Thesis), pp.

[113] Källén M., Hallberg P., Rydén M., Mattisson T.,Lyngfelt A. (2014), Combined oxides of iron, manganese and silica as oxygen carriers for chemical-looping combustion, Fuel Processing Technology 0(124), pp. 87-96

[114] Källén M., Rydén M., Mattisson T.,Lyngfelt A. (2014), Operation with Combined Oxides of Manganese and Silica as Oxygen Carriers in a 300 Wth Chemical-looping Combustion Unit, Energy Procedia 0(63), pp. 131-139

[115] Song Y.-W., Lee J.-B., Park C.-S., Hwang G.-J., Choi S.-I., Yang H.-S.,Kim Y.-H. (2006), Synthesis and redox properties of $NiO/NiAl_2O_4$ oxygen carriers for hydrogen-fueled chemical-looping combustion, Journal of Industrial and Engineering Chemistry (Seoul, Republic of Korea) 2(12), pp. 255-260

[116] Imtiaz Q., Hosseini D.,Müller C. R. (2013), Review of Oxygen Carriers for Chemical Looping with Oxygen Uncoupling (CLOU): Thermodynamics, Material Development, and Synthesis, Energy Technology 11(1), pp. 633-647

[117] Moldenhauer P., Rydén M., Mattisson T., Hoteit A., Jamal A.,Lyngfelt A. (2014), Chemical-Looping Combustion with Fuel Oil in a 10 kW Pilot Plant, Energy & Fuels 9(28), pp. 5978-5987

[118] Schmitz M., Linderholm C.,Lyngfelt A. (2014), Chemical Looping Combustion of Sulphurous Solid Fuels Using Spray-dried Calcium Manganate Particles as Oxygen Carrier, Energy Procedia 0(63), pp. 140-152